

Toward Globally Optimal State Estimation Using Automatically Tightened Semidefinite Relaxations

Frederike Dümbsen Connor Holmes Ben Agro Timothy D. Barfoot

Abstract—In recent years, semidefinite relaxations of common optimization problems in robotics have attracted growing attention due to their ability to provide globally optimal solutions. In many cases, it was shown that specific handcrafted redundant constraints are required to obtain tight relaxations and thus global optimality. These constraints are formulation-dependent and typically require a lengthy manual process to find. Instead, the present paper suggests an automatic method to find a set of sufficient redundant constraints to obtain tightness, if they exist. We first propose an efficient feasibility check to determine if a given set of variables can lead to a tight formulation. Secondly, we show how to scale the method to problems of bigger size. At no point of the process do we have to manually find redundant constraints. We showcase the effectiveness of the approach, in simulation and on real datasets, for range-based localization and stereo-based pose estimation. Finally, we reproduce semidefinite relaxations presented in recent literature and show that our automatic method finds a smaller set of constraints sufficient for tightness than previously considered.

Index Terms—Optimization and optimal control, Localization, Robot Safety, Global Optimality

I. INTRODUCTION

Many problems encountered in robotic state estimation, such as calibration and simultaneous localization and mapping (SLAM), are typically posed as nonlinear least-squares optimization problems [1, 2]. Widely adopted solvers used to tackle these problems, such as Gauss-Newton (GN) and Levenberg-Marquardt (LM), have only local, if any, convergence guarantees and may terminate in suboptimal solutions [3].

Over the past years, there has been a growing effort to exploit semidefinite relaxations of these optimization problems. Semidefinite relaxations open the door to global optimality in at least two different ways: in certain cases, a (convex) semidefinite program (SDP) (or a sequence thereof) may be solved instead of the original nonconvex problem to find the globally optimal solution [4, 5, 6, 7]. In other cases, the Lagrangian dual of the SDP offers the possibility to construct so-called ‘optimality certificates’ [8, 9] to determine the global optimality of the solutions obtained by local solvers.

The performance and feasibility of the aforementioned methods greatly depends on whether the SDP relaxation is tight. For example, the globally optimal solution to the original problem can only be extracted from the SDP solution when it is rank one, in which case the relaxation is tight [8, 5, 10]. Similarly, certifiable algorithms work only when strong duality

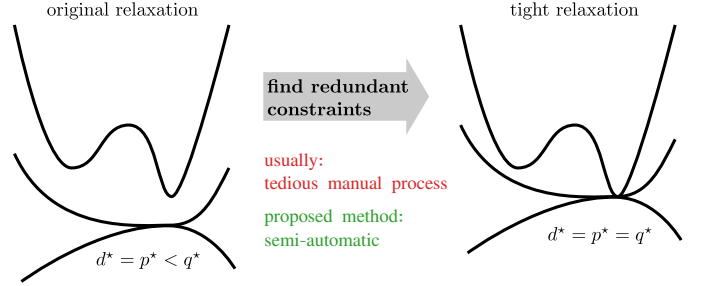


Fig. 1: The proposed method in a nutshell: we circumvent the lengthy process of finding redundant constraints to tighten a given semidefinite relaxation, using instead a sampling-based approach to automatically find all possible constraints. This allows for the quick evaluation of different formulations and substitutions of a given optimization problem, hopefully lowering the barrier for SDPs to be more widely adopted for finding globally optimal solutions to optimization problems in robotics.

obtains [11], i.e., when the cost the relaxed problem solution equals the cost of the original problem [8, 5]. Tightness can also be a computational advantage; some state-of-the-art SDP solvers, for instance, work only for problems with low-rank optimal solutions [12, 6].

One important enabler for tight relaxations has been a mathematical framework called *Lasserre’s hierarchy* [13]. Put simply, the hierarchy consists of a sequence of semidefinite relaxations where polynomial substitutions of increasing order are added to the original problem. Calling the original variable dimension d and the hierarchy order k , each level results in a N_k -dimensional SDP, with $N_k := \binom{d+k}{k}$. Astonishingly, under weak technical assumptions, any problem that can be written as a polynomial optimization problem (POP) can be ‘lifted’ to a high enough order k to allow for a tight relaxation. In theory, the required order may be infinite, but many follow-up works have shown that tightness is obtained within a few hierarchy levels only [14, 8, 15, 16]. More recently, it has been shown that many problems admit a *sparse Lasserre’s hierarchy*, meaning that only some of the N_k terms may be required at each level [17, 7].

As SDPs scale poorly with problem dimension, it is desirable to achieve tightness with as few additional higher-order substitutions as possible (ideally, with none). For this matter, it has been shown that so-called redundant constraints are paramount [8, 10, 14]. However, to this date, these constraints are usually the result of a lengthy manual search process and it is often hard to retrace how the constraints were discovered [14]. In [7], a method to find all ‘trivially satisfied’ constraints is provided, but not all of these constraints may

be necessary, and important constraints might be missed. To make matters worse, using different formulations may lead to entirely different forms and numbers of required redundant constraints. Due to the lack of a systematic method of finding the right formulation and sufficient redundant constraints, practitioners often have to spend great effort in trial-and-error reformulations. This adds significant overhead as opposed to easy-to-use local solvers, and thus may hinder the wide adoption of SDP methods in robotics.

In this paper, we provide tools that help automate the search for redundant constraints required for tightness. In particular, the proposed methods allow us to

- 1) determine, in only a few lines of code, if a problem in a given form can be tightened by adding enough redundant constraints. Notably, no manual steps for guessing the redundant constraints are required. This step is purposefully kept simple, allowing for quick evaluation of any problem in a given formulation (AUTOTIGHT).
- 2) automatically determine a set of ‘constraint templates’ that can be generalized to any number of variables, requiring again no need to explicitly model or interpret the found constraints (AUTOTEMPLATE).

The focus of AUTOTIGHT is feasibility and it should be performed on a small example problem. The focus of AUTOTEMPLATE is scalability, enabling to generalize the findings from AUTOTIGHT to problems of any size, which is a hard requirement for typically high-dimensional problems encountered in robotics.

The only prerequisite for using the provided tools is a method of randomly generating many problem setups (also called a ‘sampling oracle’ in the literature [18]). We believe that most roboticists generate such a method as part of their standard development process, and if not, can do so fairly easily in only a few lines of code.

This paper is structured as follows. We put the proposed method in context with related work in Section II. Then, we introduce mathematical preliminaries for relaxing a non-linear least-squares problem to an SDP in Section III. In Section IV, we present our method to determine the feasibility of tightening a given problem. Building on this method, in Section V we propose a scalable method for determining constraint templates that can be applied to any number of variables. We use the methods to provide novel insights on two state-estimation problems in Sections VI-B and VI-C, and on previously studied relaxations in VI-D. Finally, we test the method on real-world datasets for range-only (RO) and stereo-camera localization in Section VII and conclude in Section VIII.

II. RELATED WORK

The list of problems in robotics and computer vision that have been solved using semidefinite relaxations is long and continues to grow. In vision-based state estimation, semidefinite relaxations have been widely explored, for example to solve rotation averaging [19, 20, 21] or to perform camera pose estimation from pixel measurements [10, 22]. The first theoretical guarantees on tightness of these and other problems were given in [23, 9]. A set of analytical redundant

constraints that successfully tightens many problem instances involving rotations has been proposed in [24, 10] and used successfully in follow-up works to certify, for instance, hand-eye calibration [25] and generalized-essential-matrix estimation [26]. Follow-up works have shown that tight relaxations can be achieved for robust cost functions, too, which account for outliers [16, 8]. A great overview of many successfully tightened problems and robust cost functions is given in [7], in which a recipe for constructing trivially satisfied redundant constraints is also provided. Robotics planning and control problems have recently also seen a surge of relaxation-based methods [15, 27, 28]. Notably, specific redundant constraints (again, analytically specified) were found to be paramount for tightness in [28].

For some problems, no redundant constraints are required for tightness. For these problems, methods based on the *Burer Monteiro* approach [29] and the *Riemannian staircase* [30] have been shown to be extremely effective at finding the optimal solution with speeds competitive with efficient local solvers [4, 5, 31, 32]. Other methods have explored fast global optimality certificates of solutions of local solvers [33, 34]. To date, whenever redundant constraints are required for tightness, SDP solvers are generally too slow for real-time performance [7]. However, recent advances have shown that solvers can be significantly sped up when the optimal solution is of low rank [35, 6, 7]. More progress in finding faster SDP solvers for these convex relaxations is a requirement to enable the large-scale adoption of SDPs for robotics; another requirement is finding the necessary redundant constraints for a larger class of problems. We hope that the method proposed in this paper contributes to the latter.

Recently, a sampling paradigm has been explored in the sums-of-squares (SOS) literature to overcome some of the limitations of SDP solvers [18].¹ The authors suggest to sample feasible points of an SOS program and to solve an SDP including only a minimally required number of samples. The method thus implicitly exploits coordinate ring structure of the variety without the use of advanced concepts such as Grobner bases [36]. This solution has been picked up and shown great promise on small problems [37]. We use a similar paradigm in this paper, but instead of solving a sampling-based SDP, we use the samples to find generalizable constraints. Not only does this provide more insight into the kind of redundant constraints required to tighten standard SDP problems of a wide range of problems, it also allows us to generalize to novel, higher-dimensional problems.

III. PRELIMINARIES

A. Notation

We denote vectors and matrices by bold-face lowercase and uppercase letters, respectively. The transpose of matrix \mathbf{A} is written as \mathbf{A}^\top . The identity matrix in d dimensions is \mathbf{I}_d , and vector \mathbf{e}_d is the d -th standard basis vector (the d -th column of the identity matrix). A positive-semidefinite (PSD) matrix

¹There is a tight connection between the SOS relaxation and Lasserre’s hierarchy (also called moment relaxation in this context); a clear description of this connection is given in [21].

is written as $\mathbf{X} \succeq 0$, and we denote the space of $N \times N$ PSD matrices by \mathbb{S}_+^N . The inner product is denoted by $\langle \cdot, \cdot \rangle$, and the matrix inner product is defined as $\langle \mathbf{A}, \mathbf{B} \rangle = \text{tr}(\mathbf{A}^\top \mathbf{B})$ where $\text{tr}(\cdot)$ is the trace operator. We introduce $\text{vech}(\cdot)$ which extracts the elements of the upper-triangular part of a matrix, and divides the diagonal elements by $\sqrt{2}$. This ensures that $\langle \mathbf{A}, \mathbf{B} \rangle = \text{vech}(\mathbf{A})^\top \text{vech}(\mathbf{B})$, and is commonly used in SDP solvers [38]. We denote the inverse operation by $\text{vech}^{-1}(\cdot)$. $\mathbf{x}[k]$ denotes the k -th element of vector \mathbf{x} . For shorter notation, we use $[N]$ for the index set $\{1, \dots, N\}$.

B. Semi-definite Relaxations

In the remainder of this section, we provide theoretical background on semidefinite relaxations and duality theory necessary to understand this paper for the nonexpert reader. For an in-depth introduction to these topics we refer to [11, 3].

Most generally speaking, the subject of this paper is optimization problems of the form

$$\min_{\boldsymbol{\theta} \in \mathbb{R}^d} \{c(\boldsymbol{\theta}) \mid h_i(\boldsymbol{\theta}) = 0, i \in [N_h]\}, \quad (1)$$

where $\boldsymbol{\theta}$ is a decision variable, $c(\cdot)$ is the cost, and $h_i(\cdot)$ are equality constraints.² In robotics, the cost is most commonly a (robust) least-squares cost function, and the constraints may enforce the nature of the decision variables, such as $SO(3)$ for rotations or $SE(3)$ for poses [2].

The problems in which we are interested can be ‘lifted’ to a quadratically constrained quadratic program (QCQP). This includes, for instance, any POP; we show examples of a quartic and a rational cost function in Section VI. For such problems, we can rewrite (1) as

$$\min_{\mathbf{x} \in \mathbb{R}^N} \{f(\mathbf{x}) \mid g_i(\mathbf{x}) = 0, l_j(\mathbf{x}) = 0, i \in [N_h], j \in [N_l]\}, \quad (2)$$

where f and g_i are now quadratic in the lifted vector \mathbf{x} . The lifted vector is given by

$$\mathbf{x}^\top = [1 \quad \boldsymbol{\theta}^\top \quad z_1 \quad \dots \quad z_{N_l}], \quad (3)$$

where we have introduced $z_l := \ell_l(\boldsymbol{\theta})$, higher-order lifting functions of $\boldsymbol{\theta}$. By choosing enough of these substitutions, we can enforce that each substitution can itself be written as a quadratic constraint: $l_j(\mathbf{x}) = 0$. We have also added h in (3) as a homogenization variable, allowing constant and linear functions to be written as quadratic functions. We illustrate these concepts in the following example:

Example (stereo-1D). *Inspired by stereo-based localization problems, which typically involve rational cost functions, we propose the following pedagogical example problem:*

$$\min_{\boldsymbol{\theta}} \sum_{i=1}^N \left(\frac{1}{(\boldsymbol{\theta} - a_i)} \right)^2, \quad (4)$$

²We focus on equality constraints here for the sake of clarity. Note that inequality constraints can be added as long as they can also be written as quadratic constraints in the lifted vector and thus carried forward as quadratic inequality constraints in the relaxations. We include one example of inequality constraints in Section VI-D.

where $\boldsymbol{\theta} \in \mathbb{R}$ is the decision variable, and $a_i \in \mathbb{R}$ are known. Using the lifted vector

$$\mathbf{x}^\top = [h \quad \boldsymbol{\theta} \quad z_1 \quad \dots \quad z_N], \quad z_i = \ell_i(\boldsymbol{\theta}) := \frac{1}{\boldsymbol{\theta} - a_i}, \quad (5)$$

we can rewrite (24) in the form (2), with $f(\mathbf{x}) = \sum_{i=1}^N \mathbf{x}[2+i]^2$, and $l_i(\mathbf{x}) = \mathbf{x}[2+i]\mathbf{x}[1] - \mathbf{x}[2+i]a_i = 0$, which are both quadratic functions in the lifted variable $\mathbf{x}^\top = [1 \quad \boldsymbol{\theta} \quad z_1 \quad \dots \quad z_N]$.

Since all functions in (2) are quadratic in the lifted vector, we can now rewrite (2) as

$$\min_{\mathbf{x} \in \mathbb{R}^N} \{ \mathbf{x}^\top \mathbf{Q} \mathbf{x} \mid \mathbf{x}^\top \mathbf{A}_0 \mathbf{x} = 1, \mathbf{x}^\top \mathbf{A}_i \mathbf{x} = 0, i \in [N_A] \}, \quad (6)$$

where \mathbf{Q} and $\mathbf{A}_i, i \in [N_A]$ are the cost and constraint matrices, respectively, and $N_A = N_h + N_l$. The matrix \mathbf{A}_0 enforces the homogenization variable through the constraint $\mathbf{x}[1]^2 = 1$.³ We call the constraints in (6) the ‘primary constraints’.

Example (stereo-1D, cont’d). *The cost and constraints matrices for the toy stereo problem are zero except for $\mathbf{Q}[i, i] = 1$ for $i = 3 \dots N+2$ and $\mathbf{A}_i[1, 2+i] = \mathbf{A}_i[2+i, 1] = -a_i$ and $\mathbf{A}_i[2, 2+i] = \mathbf{A}_i[2+i, 2] = 1$.*

Problem (6) is a QCQP. Its solution space, defined by a set of polynomial equality constraints, defines a real algebraic variety, which is a central object of the field of algebraic geometry. This is by itself an active area of research, with methods existing for finding, for example, the minimal set of constraints to uniquely define a variety [36]. For the proposed paper, no knowledge of these advanced concepts is required as we take a numerical approach rather than an algebraic approach to describe the varieties. For the interested reader, we do include some references to the algebraic geometry perspective in footnotes.

Because (6) is, in general, NP-hard to solve, a common strategy is to relax the problem to a SDP by introducing $\mathbf{X} := \mathbf{x}\mathbf{x}^\top$, which can be enforced using $\mathbf{X} \succeq 0, \text{rank}(\mathbf{X}) = 1$, where the semidefinite constraint is convex while the rank constraint is not. We can solve the following standard SDP, also called the primal relaxation of (6):

$$\min_{\mathbf{X} \in \mathbb{S}_+^N} \{ \langle \mathbf{Q}, \mathbf{X} \rangle \mid \langle \mathbf{A}_0, \mathbf{X} \rangle = 1, \langle \mathbf{A}_i, \mathbf{X} \rangle = 0, i \in [N_A] \}, \quad (7)$$

which is the rank-relaxation of (6) (i.e., we relax the $\text{rank}(\mathbf{X}) = 1$ constraint).

C. Duality Theory and Global Optimality

The SDP problem can be used in several ways to make claims about the global optimality of candidate solutions. Let us denote by \mathbf{X}^* the solution of (7) and its associated cost by $p^* := \langle \mathbf{Q}, \mathbf{X}^* \rangle$. If \mathbf{X}^* has rank one, then it can be factored as $\mathbf{X}^* = \mathbf{x}^* \mathbf{x}^{*\top}$ and \mathbf{x}^* is the optimal solution to (6) with $q^* := f(\mathbf{x}^*) = p^*$. This leads us to the first form of tightness used in this paper.

³Technically, the first element of \mathbf{x} may thus take the value -1 , but this does not pose a problem as the whole vector can then be simply negated.

Definition 1 (Rank-tightness of the SDP relaxation). *We call the SDP relaxation (7) rank-tight if its optimal solution \mathbf{X}^* has rank one.*

SDPs also enjoy a well-understood duality theory, which makes them great candidates for so-called ‘optimality certificates’. The Lagrangian dual problem of (7) is given by

$$d^* = \max_{\rho, \boldsymbol{\lambda}} \{-\rho \mid \mathbf{H}(\rho, \boldsymbol{\lambda}) := \mathbf{Q} + \rho \mathbf{A}_0 + \sum_{i=1}^{N_A} \lambda_i \mathbf{A}_i \succeq 0\}, \quad (8)$$

where $\rho, \boldsymbol{\lambda} \in \mathbb{R}^{N_A}$ are the Lagrangian dual variables corresponding to \mathbf{A}_0 and $\mathbf{A}_i, i \in [N_A]$, respectively. It is well known that we always have $d^* \leq p^* \leq q^*$ (see left graph of Figure 1 for a graphical depiction). In what follows, we will also make the assumption that $d^* = p^*$ which holds under common constraint qualifications such as *Slater’s condition* [11].

We can use the dual problem to, instead of solving the primal SDP and checking the rank of the solution, certify a local candidate solution $\hat{\mathbf{x}}$. Indeed, using the Karush-Kuhn-Tucker (KKT) conditions of (8), it is well-known (see e.g., [39]) that a solution candidate $\hat{\mathbf{x}}$ is globally optimal if there exist $\hat{\rho}, \hat{\boldsymbol{\lambda}}$ such that

$$\begin{cases} \mathbf{H}(\hat{\rho}, \hat{\boldsymbol{\lambda}}) \hat{\mathbf{x}} = \mathbf{0}, \\ \mathbf{H}(\hat{\rho}, \hat{\boldsymbol{\lambda}}) \succeq 0. \end{cases} \quad (9a) \quad (9b)$$

If these two conditions hold, we have *strong duality*, meaning that $d^* = p^* = q^*$ (right plot of Figure 1). If we do not have strong duality, the above conditions cannot be jointly satisfied and we cannot make claims about the global optimality of a candidate solution. Therefore, we introduce the notion of *cost-tightness*, a weaker form of tightness than rank-tightness,⁴ which allows for candidate solutions to be certified:

Definition 2 (Cost-tightness of the SDP relaxation). *We call the SDP relaxation (7) cost-tight if $d^* = p^* = q^*$.*

Both forms of tightness may be useful in practice: when we have rank-tightness, we can solve the SDP and derive the optimal value of the QCQP from it. When the SDP is prohibitively large, or when only cost-tightness is attained, one may instead resort to a local solver and certify the solution candidate using Lagrangian duality. For completeness, we also mention that in some cases, one may extract a solution estimate from a higher-rank solution of the SDP in a procedure called ‘rounding’, see e.g., [5]. This typically consists of extracting the dominant eigenvector from \mathbf{X}^* , and projecting it to the feasible set of (1). Note that in this case there are no guarantees on the quality of the solution and cases have been reported where the obtained estimate is far from the global optimum [40].

We have seen that either rank- or cost-tightness are necessary for efficiently obtaining or certifying globally optimal solutions, respectively. The remaining question is how one may increase the tightness of a given problem. This leads to the notion of redundant constraints, as explained next.

D. Redundant Constraints

Redundant constraints can be added to (2) without changing its feasible set (thus the name ‘redundant’).⁵ While the constraints are redundant for the QCQP, they may, however, change the feasible region of the SDP. In particular, redundant constraints typically reimpose structure on \mathbf{X} that is lost when relaxing the rank-one constraint. For example, if the lifted vector is $\mathbf{x}^\top = [1 \ \theta \ \theta^2 \ \theta^3]$, then

$$\mathbf{X} = \mathbf{x} \mathbf{x}^\top = \begin{bmatrix} 1 & \theta & \theta^2 & \theta^3 \\ \star & \theta^2 & \theta^3 & \theta^4 \\ \star & \star & \theta^4 & \theta^5 \\ \star & \star & \star & \theta^6 \end{bmatrix}, \quad (10)$$

which has a very clear structure (it is a Hankel matrix, as is always the case for semidefinite relaxations of scalar polynomial problems [41]) that might be lost in the relaxation. The lifting constraints (in this case, $\mathbf{x}[3] = \mathbf{x}[2]^2$ and $\mathbf{x}[4] = \mathbf{x}[3]\mathbf{x}[2]$) and symmetry of the solution take care of constraining all terms of degree 0 to 3 as well as θ^5 , but nothing directly enforces that the elements corresponding to θ^4 in the variable \mathbf{X} are equal. In this case, we can add the redundant constraint corresponding to $(\mathbf{x}[3]^2 = \mathbf{x}[2]\mathbf{x}[4])$ to enforce exactly that. Redundant constraints can often be hard to find — as our continued example illustrates.

Example (stereo-1D, cont’d). *A simple computation shows that*

$$z_i - z_j = \frac{1}{\theta - a_i} - \frac{1}{\theta - a_j} = (a_i - a_j)z_i z_j, \quad (11)$$

which holds for any $i \neq j$ and z_i, z_j constructed using the lifting functions $\ell_i(\theta)$ introduced in (5). This shows that equation (11), which is quadratic in the elements of \mathbf{x} , is redundant in (2), but non-redundant in the QCQP. It can be added to the QCQP with matrices \mathbf{A}_{ij} ; $\mathbf{A}_{ij}[1, i] = \mathbf{A}_{ij}[i, 1] = 1$, $\mathbf{A}_{ij}[1, j] = \mathbf{A}_{ij}[j, 1] = -1$, $\mathbf{A}_{ij}[i, j] = \mathbf{A}_{ij}[j, i] = (a_i - a_j)$, for all $i, j \in [N], i \neq j$.

Because they impose more structure on \mathbf{X} , redundant constraints may have the effect of reducing the rank of \mathbf{X} , and thus improve the tightness of the relaxation. However, finding the right form and number of redundant constraints can be a tedious process, especially as the dimension of the problem increases. The present paper circumvents this process by proposing a numerical method to find all available redundant constraints, as we explain next.

IV. DETERMINING FEASIBILITY OF TIGHTENING (AUTOTIGHT)

In this Section, we present our method to determine whether a problem in a given form can be tightened, adding all possible redundant constraints without having to manually find or interpret them.

⁵Speaking in terms of algebraic geometry, the redundant constraints do not change the algebraic variety that is defined as the solution space.

⁴It is straightforward to see that rank-tightness implies cost-tightness.

A. Setting up the Nullspace Problem

At the core of the presented method is the idea that all of the constraint matrices \mathbf{A}_i lie in the nullspace of the linear subspace spanned by the feasible points. Indeed, assume we can generate feasible samples $\boldsymbol{\theta}^{(s)}$, and therefore also a set of lifted samples $\mathcal{X} = \{\mathbf{x}^{(1)}, \dots, \mathbf{x}^{(N_s)}\}$ with $\mathbf{x}^{(s)}$ constructed using the *known* lifting functions ℓ .⁶ Then, for any valid constraint \mathbf{A}_i (whether primary or redundant), we must have

$$\langle \mathbf{A}_i, \mathbf{X}^{(s)} \rangle = \text{vech}(\mathbf{A}_i)^\top \text{vech}(\mathbf{X}^{(s)}) = 0, \quad (12)$$

with $\mathbf{X}^{(s)} := \mathbf{x}^{(s)}\mathbf{x}^{(s)\top}$. This must hold for all samples $\mathbf{x}^{(s)}$. Defining the data matrix $\mathbf{Y} = [\text{vech}(\mathbf{X}^{(1)}) \dots \text{vech}(\mathbf{X}^{(N_s)})] \in \mathbb{R}^{n \times N_s}$, the set of ‘learned’ constraints, \mathcal{A}_l , is the left nullspace basis of \mathbf{Y} :

$$\mathcal{A}_l = \{\mathbf{A}_1, \dots, \mathbf{A}_{N_n}\} = \{\text{vech}^{-1}(\mathbf{a}_i) \mid \mathbf{a}_i^\top \mathbf{Y} = \mathbf{0}\}. \quad (13)$$

In other words, each nullspace basis vector corresponds to one (vectorized) constraint matrix. Therefore, finding all possible constraints is a standard nullspace problem. The dimension of the nullspace, N_n , corresponds to the total number of constraints. Note that we have exploited the fact that $\mathbf{X}^{(s)}$ and \mathbf{A}_i are symmetric in using the half-vectorization operator, which reduces the problem size to $n := \frac{N(N+1)}{2}$.

By definition, all the constraints found through (13) are linearly independent when operating in matrix form. When using the constraints in (6), however, the constraints may become dependent; in other words, the method finds both primary and redundant constraints.

Sometimes, it may be desirable to enforce some of the basis vectors to be known, for example to enforce the primary constraints. We denote the set of constraints to be enforced by $\mathcal{A}_k = \{\tilde{\mathbf{A}}_1, \dots, \tilde{\mathbf{A}}_{N_k}\}$. Completing the nullspace basis is as simple as appending the known constraints to the data matrix \mathbf{Y} :

$$\mathbf{Y} = [\text{vech}(\mathbf{X}^{(1)}) \dots \text{vech}(\mathbf{X}^{(N_s)}) \text{vech}(\tilde{\mathbf{A}}_1) \dots \text{vech}(\tilde{\mathbf{A}}_{N_k})]. \quad (14)$$

By definition, the left nullspace vectors of \mathbf{Y} will then be orthogonal to the known constraints.

To find a valid nullspace basis, we need to have at least $r = n - N_n$ samples, with n the number of rows of \mathbf{Y} , N_n the nullspace dimension, and r the rank of \mathbf{Y} . However, since r is not known a priori, a viable strategy is to randomly generate $N_s > n$ samples.⁷ This ensures that the data matrix is rank-deficient, and the nullspace basis can be calculated using the permuted QR decomposition, as we explain next.

B. Sparse Basis Retrieval

We know that the constraint matrices are typically sparse, since they usually involve a subset of variables. Can we

ensure that the learned constraints are expressed in a basis that encourages sparsity? Sparsity is good not only for lower runtime and memory consumption of SDP solvers, but also because sparser matrices are more easily interpretable, should we want to determine what the algebraic expression of the constraints is.⁸ Unfortunately, finding the sparsest nullspace basis is a NP-hard problem [42]. However, we can use a pivoted, or rank-revealing, QR decomposition [43] to find the left nullspace of the data matrix and to induce sparsity in the resulting basis vectors. We found the resulting constraints to be sufficiently sparse for downstream operations, and in both applications covered in Section VI, some basis vectors are even as sparse as analytically constructed constraints. Other matrix decomposition alternatives, such as the singular value decomposition (SVD), were empirically found to exhibit less sparsity.

The pivoted QR decomposition returns a decomposition of the form [43]

$$\mathbf{Y}^\top \mathbf{P} = \mathbf{Q}\mathbf{R} = \mathbf{Q} \begin{bmatrix} \mathbf{R}_1 & \mathbf{R}_2 \\ \mathbf{0} & \mathbf{0} \end{bmatrix}, \quad (15)$$

where \mathbf{P} is a $n \times n$ permutation matrix ensuring that the diagonal of \mathbf{R} is non-increasing, \mathbf{Q} is $N_s \times N_s$ and orthogonal, \mathbf{R}_1 is upper-diagonal with dimensions $r \times r$, and \mathbf{R}_2 is of size $r \times N_n$. The nullspace basis vectors \mathbf{a}_i are then given by

$$[\mathbf{a}_1 \dots \mathbf{a}_{N_n}] = \mathbf{P} \begin{bmatrix} \mathbf{R}_1^{-1} \mathbf{R}_2 \\ -\mathbf{I}_{N_n} \end{bmatrix}. \quad (16)$$

Note that when using the permuted QR decomposition, the obtained basis vectors are linearly independent, but not necessarily orthogonal to each other, as would be the case with an SVD, for example. However, we found that the increased sparsity was of higher importance, both for computational speed and interpretability, than orthogonality.

C. Determining Tightness

All considerations so far are independent of the cost function and only depend on the chosen substitutions and primary constraints. To determine if the relaxation is tight, we need to define the cost, *i.e.*, form the matrix \mathbf{Q} in (6). In general, tightness may be a function of both the noise magnitude [39] and the sparsity of the measurement graph [9]. The proposed method takes both into account as we fix \mathbf{Q} and then determine the tightness (and required redundant constraints) for this particular choice.

We determine cost-tightness by comparing the cost of the dual problem with the cost of a candidate global solution. The candidate global solution is found by running an off-the-shelf local solver initialized at the ground-truth state, which we expect to be close to the optimal solution for low-enough noise. Indeed, this strategy allowed us to find the global minimum almost always for the noise regimes considered in Section VI. If not, we regenerate a new random setup and start again.⁹ We compute the relative duality gap (RDG) between

⁶Note that we can also allow for unknown or numerical lifting functions, as long as a sampler of \mathbf{x} is available.

⁷The emphasis here is on random; this ensures that all samples are linearly independent with probability one, to yield what is also called ‘generic’ samples [18]. Intuitively speaking, when using generic samples one can ensure that properties derived from the samples hold for the entire variety.

⁸We reiterate that interpretability is not necessary, but it may be beneficial for scalability and for gaining a better understanding of a given problem.

⁹As soon as we find that the cost of the candidate solution is equal to the dual cost (up to numerical tolerance), we know that it corresponds to the global minimum, because of duality theory [11].

the cost of this local solution, called \hat{q} , and the optimal dual cost d^* through $(\hat{q} - d^*)/q^*$, and report cost-tightness if the RDG is below a fixed threshold (see Section VI-A).

To determine rank-tightness, we calculate the eigenvalues of the solution \mathbf{X} , and take the ratio of the first to the second-largest eigenvalue, called the singular-value ratio (SVR) in what follows. If the ratio is larger than a fixed value (see Section VI-A) we report that the solution is rank one.

D. Summary

We conceptualize the algorithm AUTOTIGHT, which is defined by the successive application of IV-A to IV-C, by the gray boxes in Figure 2. In summary, we randomly generate $N_s > n$ samples of the half-vectorized feasible points and compute a nullspace basis of the samples, which gives us all possible constraints. We then determine if the SDP relaxation is rank- or cost-tight when using all found constraints. There are three possible outcomes of this method:

- 1) The problem cannot be tightened. Knowing this, no additional effort has to be spent in trying to find redundant constraints for this formulation. Either a new formulation can be tried — adding for instance (a subset of) higher-order Lasserre terms [13] — or the SDP can be used in conjunction with rounding, for example as an initialization for a local solver.
- 2) The problem can be tightened without any redundant constraints, or with few redundant constraints that are interpretable. By interpretable we mean that the algebraic form can be derived directly from each matrix — we will see such examples in Section VI, Figure 4. In this case, constraints matrices can be efficiently created analytically, as in classical methods [7].
- 3) The problem can be tightened, but with many redundant constraints. In this case, the method presented so far would have to be reapplied to any new problem instance in order to find the required redundant constraints, which does not scale to the large problem sizes typically encountered in robotics.

We will revisit the first two outcomes in the experiments in Section VI. The next section deals with the third outcome: We present a method that finds what we call *constraint templates* — particular patterns that can be applied to any number and combination of variables of particular types.

V. GENERATING SCALABLE CONSTRAINTS (AUTOTEMPLATE)

The method AUTOTIGHT finds, for a given problem instance, whether the problem can be tightened. However, tightness will most likely be lost as we increase the problem size if we do not add the redundant constraints corresponding to new variables. Applying AUTOTIGHT is prohibitively expensive as the dimensionality of the problem increases, due to the cubic complexity of the QR decomposition. We thus present AUTOTEMPLATE, an extended version of AUTOTIGHT that is more scalable.

A. Algorithm Overview

Thankfully, while problems in robotics tend to be high-dimensional, they usually only exhibit a few different variable types. For example, in SLAM, the only variable types are robot poses and landmark positions [2]. We would expect the constraints relating instances from the same variable types to be repeatable; for example, all constraints that touch one pose should hold for all other poses too.

The additions to AUTOTIGHT to make it scalable are shown in the white and dashed boxes in Figure 2. Initially, we still operate on a small example problem; however, the output of AUTOTEMPLATE are templates that can be scaled to any problem size. The method consists of the following steps:

- 1) We set up the nullspace problem as explained in IV-A, but now we only operate on one variable group at a time, which leads to much smaller nullspace problems. At this point, we may also factor out parameters — variables of our problem that are known a priori, such as landmark positions in localization problems. We explain this in more detail in V-B.
- 2) We compute the nullspace vectors as in Section IV-B, but interpret the resulting basis vectors as constraint templates.
- 3) We apply these templates to all other variables of the same group(s) as outlined in V-C.
- 4) We check tightness of the problem as in Section IV-C. If the problem is tight, we return all the learned constraints as templates. If it is not, we go back to step 1).

As opposed to AUTOTIGHT, AUTOTEMPLATE requires some manual input by the user: defining the variable groups and parameters, and their order of consideration. Compared to having to manually find and define required redundant constraints, this is relatively simple. We give examples of variable selections for the examples studied in this paper in Table II in Section VI, which likely extend to most problems encountered in robotics.

B. Factoring Out Parameters

For some problems, constraints may depend on parameters that are known a priori. In the stereo-1D example presented in Section III, and in the stereo-based localization problem presented in Section VI-C, for example, the constraints depend on the known landmark coordinates. Because of this, the learned constraints may not be applicable to other random setups. To overcome this problem, we treat such quantities as ‘parameters’ and append them to the samples of feasible points. Let $\mathbf{p} \in \mathbb{R}^{N_p}$ be the vector of N_p parameters, for instance the coordinates of landmarks, and let $\kappa(\mathbf{p}) : \mathbb{R}^{N_p} \rightarrow \mathbb{R}^K$ be a chosen lifting function that outputs K lifted elements. This lifting function needs to be chosen generally enough so that it encompasses all expected dependencies. In the absence of prior knowledge, we suggest monomials up to the maximum degree of θ in (2). For example, for up to quadratic substitutions we would use

$$\kappa(\mathbf{p}) = \text{vech} \left(\begin{bmatrix} 1 \\ \mathbf{p} \end{bmatrix} \begin{bmatrix} 1 & \mathbf{p}^\top \end{bmatrix} \right). \quad (17)$$

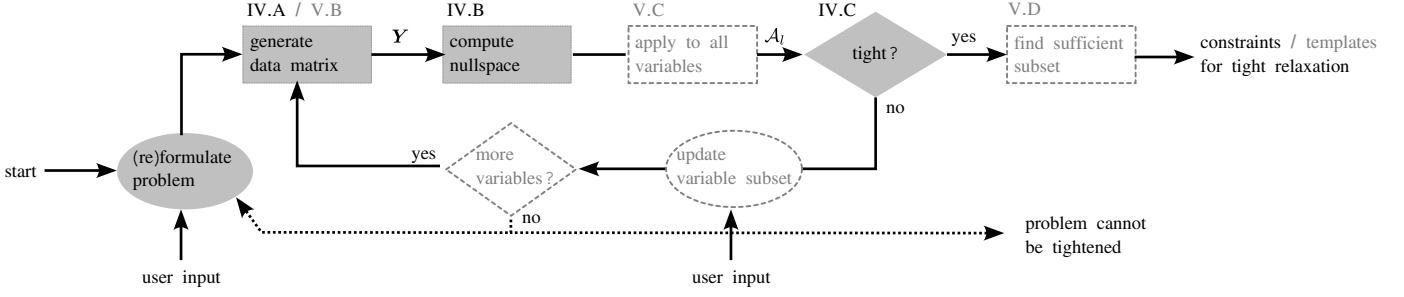


Fig. 2: Overview of proposed algorithm to automatically find constraints or templates. Highlighted in gray and white, respectively, are the components of AUTOTIGHT and AUTOTEMPLATE. The two stages where (minor) user input is required are shown in the bottom.

Using the lifted parameters, we modify each feasible sample to include the parameter dependencies, leading to the ‘augmented’ feasible sample $\bar{z}^{(s)} \in \mathbb{R}^{\bar{n}}$ of size $\bar{n} := nK$:

$$\bar{z}^{(s)} := \text{vech} \left(\mathbf{x}^{(s)} \mathbf{x}^{(s)\top} \right) \otimes \kappa(\mathbf{p}). \quad (18)$$

The augmented data matrix $\bar{\mathbf{Y}} \in \mathbb{R}^{\bar{n} \times \bar{N}_s}$ is given by

$$\bar{\mathbf{Y}} = [\bar{\mathbf{z}}_1 \quad \cdots \quad \bar{\mathbf{z}}_{\bar{N}_s}], \quad (19)$$

where we note that the number of samples \bar{N}_s now has to be chosen as to ensure that $\bar{\mathbf{Y}}$ is rank-deficient. We denote the left nullspace basis vectors of (19) by $\bar{\mathbf{a}}_l \in \mathbb{R}^{\bar{n}K}$, with $l \in [\bar{N}_n]$. We call these basis vectors ‘templates’ because we will apply them to new variable sets, and in particular, scale them to any required problem size, as we explain next.

C. Applying Templates

Conceptually speaking, applying the templates means repeating each constraint for each possible combination of the variables that it involves. For example, if one constraint matrix involves one position and two different landmarks, then we repeat the constraint for each position and each possible pair of landmarks per position. To facilitate this operation programmatically, we have created an easy-to-use tool to generate sparse matrices using variable names for indexing.¹⁰ That way, applying constraints to all possible variables simply means creating duplicates of a given constraint, and then renaming the variables that it touches.

If parameters were factored out as explained in V-B, then they need to be factored back in before solving the SDP, using the current parameter realization. We introduce the operator $\text{mat}(\cdot)$, which folds the augmented basis vector $\bar{\mathbf{a}}_l$ (which we recall has nK dimensions, with K the number of lifted parameters) column-wise into a $n \times K$ matrix. Then, *factoring in* the parameters of a specific parameter realization $\mathbf{p}^{(s)}$ can be written as

$$\mathbf{a}_l = \text{mat}(\bar{\mathbf{a}}_l) \kappa(\mathbf{p}^{(s)}), \quad (20)$$

where the output $\mathbf{a}_l \in \mathbb{R}^n$ is now a problem-specific vectorized constraint that can be converted to the corresponding constraint matrix $\mathbf{A}_l = \text{vech}^{-1}(\mathbf{a}_l)$. We return to the stereo-1D example to illustrate these concepts:

Example (stereo-1D, cont’d). Looking at (11), we see that the redundant constraints depend on the problem parameters \mathbf{a}_i : we have $\mathbf{p}^\top := [a_1 \cdots a_N] \in \mathbb{R}^N$ and $K := N$. Because the lifting constraints $l_i(\mathbf{x})$ are linear in θ , we introduce the lifting function $\kappa(\mathbf{p}) := [1 \ a_1 \ a_2 \ \cdots \ a_N]^\top$. We define the following set of variable groups: $\{(1, \theta, z_1, a_1), (1, \theta, z_1, a_1, z_2, a_2), \dots\}$. When imposing the known substitution constraints, we would not find any additional constraints at the first level. At the second level, however, each augmented sample would be of the form:

$$\bar{\mathbf{z}}^\top := [1 \ \theta \ z_1 \ z_2 \ \theta^2 \ \theta z_1 \ \theta z_2 \ z_1^2 \ z_1 z_2 \ z_2^2] \otimes [1 \ a_1 \ a_2], \quad (21)$$

where we have dropped superscript (s) for better readability. Clearly, the redundant constraints would now be in the nullspace of the augmented data matrix, as we have:

$$0 = \bar{\mathbf{a}}_1^\top \bar{\mathbf{z}} = [\alpha_1^\top \ \alpha_2^\top \ \alpha_3^\top] \bar{\mathbf{z}}, \quad (22)$$

for any $\bar{\mathbf{z}}$, where we have introduced

$$\begin{aligned} \alpha_1^\top &= [0 \ 0 \ 1 \ -1 \ 0 \ 0 \ 0 \ 0 \ 0 \ 0], \\ \alpha_2^\top &= [0 \ 0 \ 0 \ 0 \ 0 \ 0 \ 0 \ 0 \ 1 \ 0], \\ \alpha_3^\top &= [0 \ 0 \ 0 \ 0 \ 0 \ 0 \ 0 \ 0 \ 0 \ -1]. \end{aligned} \quad (23)$$

Note that the template $\bar{\mathbf{a}}_1$ does not depend on the landmarks anymore. This template can be applied to any variables by changing the labels as explained in Section V-C. Given also new realizations of parameters $\mathbf{p}^{(t)}$ corresponding to the new variables, we can create the corresponding constraint matrix:

$$\begin{aligned} \mathbf{a}_1^{(t)} &= \text{mat}(\bar{\mathbf{a}}_1) \mathbf{p}^{(t)} = [\alpha_1 \ \alpha_2 \ \alpha_3] \begin{bmatrix} 1 \\ a_1^{(t)} \\ a_2^{(t)} \end{bmatrix}, \\ \mathbf{A}_1^{(t)} &= \text{vech}^{-1}(\mathbf{a}_1^{(t)}). \end{aligned} \quad (24)$$

D. Reducing the Number of Constraints

Even when using the efficient sparse representation, applying the templates to all other possible combinations of variables can become the computational bottleneck of the problem. However, in practice not all of the found templates are actually necessary for tightness. Therefore, we suggest to prune the found templates before applying them to large problem sizes. In order to do that, we proceed as follows.

¹⁰The code is available as an open-source package at https://github.com/utiasASRL/poly_matrix.

Assume we have found a set of learned constraints \mathcal{A}_l for which the problem is (at least) cost-tight. Then, we can solve the following optimization problem in an attempt to sort the constraints by their importance for tightness:

$$\begin{aligned} & \min_{\lambda, \rho} \|\lambda\|_1 \\ \text{s.t. } & \mathbf{H}(\rho, \lambda) \succeq 0 \\ & \mathbf{H}(\rho, \lambda) \hat{\mathbf{x}} = \mathbf{0}, \end{aligned} \quad (25)$$

where $\|\cdot\|_1$ denotes the L_1 -norm, \mathbf{H} is defined as in (8) (with the learned matrices substituted for \mathbf{A}_k) and $\hat{\mathbf{x}}$ is the optimal solution of (6), found as explained in IV-C. Intuitively, Problem (25) finds a sparse set of dual variables required for cost-tightness, as the L_1 -norm promotes sparsity. By ordering the learned constraints by decreasing magnitude of λ and adding them one by one, we find which subset of constraints is sufficient for cost-tightness. This problem naturally lends itself to a bisection-like algorithm, where we try using all and no redundant constraints, at first, and then continue trying cutting the number of constraints in half. We terminate when the considered interval is of size one. At that point, we use only these constraints as templates, which significantly reduces the computation cost of all downstream operations, as shown in Section VI.

As another pruning step, we also make sure that all constraints are linearly independent after applying templates to other variables. For this purpose, we use the same rank-revealing QR decomposition as in IV-B but keep only the valid range-space basis vectors. Because of the sparsity of the constraints, this adds no significant cost.

E. Summary

To summarize, AUTOTEMPLATE generates scalable templates by iteratively finding the nullspace basis of smaller subsets of variable groups. We stop when the templates lead to a tight relaxation after applying them to all variable groups in a given example problem. Then, we find a subset of constraints sufficient for tightness, which can be used as templates for any new problem of the same type. When constraints depend on problem parameters, such as landmark coordinates, we also suggest a method to factor out this dependency and learn ‘augmented’ templates instead.

VI. SIMULATION RESULTS

We show the effectiveness of the proposed method on a variety of robotics problems encountered in real-world applications. An overview of all problems considered in this Section is given in Table I.

First, we perform an in-depth analysis of two example applications, providing new insights on the tightness of their relaxations. The first application is range-only localization with fixed and known landmarks, as encountered in ultra-wideband (UWB)-based localization [44, 45] or WiFi- or Bluetooth-based indoor localization [46]. We evaluate two different formulations, one of which requires redundant constraints while the other one does not. In this example, we find

TABLE I: Overview of the considered problems, their tightness and whether there are redundant constraints. Highlighted in red are formulations that were found to be non-tight.

Problem	lifting function	redundant constr.	cost-tight	rank-tight
range-only localization	\mathbf{z} (27)	no	yes	yes
	\mathbf{y} (28)	yes	yes	yes
stereo pose estimation	\mathbf{u} (32)	yes	no	no
	$\mathbf{u}, \mathbf{u} \otimes \mathbf{t}$	yes	yes	no
point-point registration [10] (PPR)	none	no	yes	yes
point-line registration [10] (PLR)	none	yes	yes	yes
robust point-cloud registration [7] (rPPR)	$\boldsymbol{\theta} \otimes \boldsymbol{\theta}$	yes	no	no
	$\boldsymbol{\theta} \otimes \mathbf{w}$	yes	yes	no
robust absolute pose estimation [7] (rPLR)	$\boldsymbol{\theta} \otimes \boldsymbol{\theta}$	yes	no	no
	$\boldsymbol{\theta} \otimes \mathbf{w}$	yes	yes	no

constraints are interpretable and we can derive their algebraic expressions.

The second application is the estimation of the pose of a stereo camera by minimizing the reprojection error of known landmarks, which refer to as stereo localization. The reprojection error can be used to model Gaussian noise on pixel measurements [47]. To the best of our knowledge, this problem has not been successfully relaxed to a tight SDP before, with common solutions typically resorting to the back-projection error [48, 16] (*i.e.*, the error is assumed Gaussian in Euclidean space). Closest to our solution is [19], where a branch-and-bound method in combination with a (non-tight) semidefinite relaxation is used to minimize the reprojection cost. Instead, we use the proposed methods to 1) find a new formulation of the problem that can be tightened using automatically-determined constraints obtained by AUTOTIGHT, and 2) use AUTOTEMPLATE to generate templates that can be scaled to new problem instances.

Finally, we select representative examples from multimodal registration [10] and robust estimation [7], and verify their tightness results using our method.

A. Hyperparameters

Throughout the experiments, we keep the following parameters fixed.

When learning the constraints, we oversample the data matrix \mathbf{Y} by 20% to improve conditioning of the nullspace problem. For the SDP solver, we use MOSEK [38] interfaced through `cvxpy` [49, 50], fixing the tolerances of primal and dual feasibility, as well as the relative complementary gap to 10^{-10} and the tolerance of infeasibility to 10^{-12} . For finding the minimal set of constraints (Section V-D), we set the relative gap termination to 10^{-1} to allow even for inaccurate solutions to be returned (as the output is only used for ordering the constraints).

In terms of local solvers, we use the off-the-shelf `pymanopt` [51] solver for all problems in Section VI-D, using the conjugate gradient optimizer and for stopping criteria 10^{-6} in gradient norm and 10^{-10} in step size. When inequality

constraints are present in the QCQP, we use the log-sum-exp function described in [52, §4.1] with $\rho = 10$ and $u = 10^{-3}$. For RO localization, we use the `scipy` implementation of the BFGS solver, and our custom GN implementation, respectively, with the same stopping criteria as for `pymanopt`.

A problem is considered cost-tight when its RDG is below 0.1%. It is considered rank-tight when the SVR is above 10^7 .

Parameters that change for each problem, such as the considered noise levels, variable groups, and toy problem sizes, are summarized in Table II. We use fully connected measurement graphs for all considered problems.¹¹

B. Range-Only Localization

1) *Problem Statement:* The goal of RO localization is to estimate the position of a moving device over time, given range measurements to fixed and known anchors. We call the anchor points $\mathbf{m}_k \in \mathbb{R}^d$ with $k \in [N_m]$ and the position at time t_n is denoted $\boldsymbol{\theta}_n \in \mathbb{R}^d$, with $n \in [N]$. We use $d = 3$ in all of the experiments. We use the following common formulation of the problem [40]

$$\min_{\{\boldsymbol{\theta}_n\}_{n=1}^N} \sum_{n,k \in \mathcal{E}} \left(d_{nk}^2 - \|\mathbf{m}_k - \boldsymbol{\theta}_n\|^2 \right)^2, \quad (26)$$

where \mathcal{E} is the edge set of a measurement graph, with an edge between position n and anchor k if their distance d_{nk} has been measured.¹²

Problem (26) is quartic in the unknowns, and thus may contain multiple local minima [34]. However, by introducing substitutions that are quadratic in $\boldsymbol{\theta}_n$, it can be lifted to a QCQP, making it a candidate for SDP relaxation. We study two such substitutions. First, looking at the cost of (26), we see that the substitution

$$z_n := \|\boldsymbol{\theta}_n\|^2 \in \mathbb{R} \quad (27)$$

is enough to make the problem quadratic in the lifted vector $\mathbf{x}^\top = [h \quad \boldsymbol{\theta}^\top \quad z_n]$. The same substitution was used in [34] and was shown to require no redundant constraints for tightness. This substitution (28) is also called a *sparse* Lasserre substitution [17] substitution. Here, we also study the more methodological (dense Lasserre) substitution that introduces all quadratic terms of $\boldsymbol{\theta}_n$, or in other words:

$$\mathbf{y}_n := \text{vech}(\boldsymbol{\theta}_n \boldsymbol{\theta}_n^\top) \in \mathbb{R}^{d(d+1)/2}. \quad (28)$$

2) Determining Feasibility of Tightening (AUTOTIGHT):

We start by using AUTOTIGHT to evaluate the two different substitutions, on a small example problem, defined in Table II.

The data matrix \mathbf{Y} introduced in Section IV-A exhibits a well-separated nullspace for both substitutions, as can be seen in Figure 3. We can see immediately that the z_n substitution leads to a small nullspace ($N_n = 3 = N$), corresponding exactly to the number of substitutions. The substitution \mathbf{y}_n , on the other hand, leads to a nullspace that includes more than just the substitution variables ($N_n = 60 = 20N$), which shows the existence of redundant constraints.

¹¹This means that we assume that at each pose, all landmarks are observed.

¹²Note that it is straight-forward to include a motion prior in (26), such as a constant-velocity prior, as shown in [34]. Such priors are typically up to quadratic in the unknowns, thus not requiring any special treatment when it comes to constraints, and are omitted for simplicity.

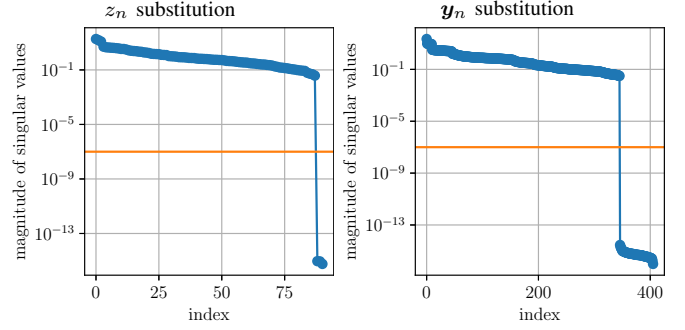


Fig. 3: Singular value spectrum of the data matrix for RO localization. The singular values below the threshold (in orange) correspond to the nullspace basis vectors. For the substitution z_n (27) (left plot), we find 3 basis vectors, however, for the substitution \mathbf{y}_n (28) (right plot) we find 20 basis vectors.

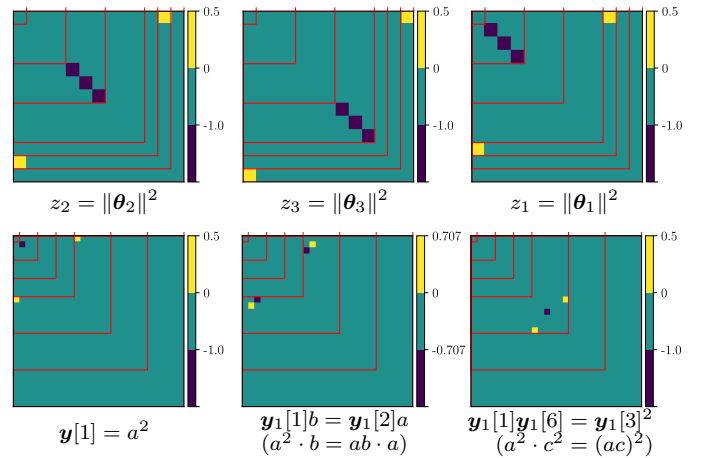


Fig. 4: Examples of learned constraint matrices for z_n substitution (top) and the \mathbf{y}_n substitution (bottom) of RO localization. Shown below each matrix are the algebraic identities that the matrices enforce. For simplicity, we call $\boldsymbol{\theta}_1^\top = [a \quad b \quad c]$.

We show the three found constraint matrices for the z_n substitution in the first row of Figure 4. Interestingly, the three automatically found matrices correspond exactly to the three substitution formulas (shown below each matrix).¹³ The second row of Figure 4 shows three example matrices for the \mathbf{y}_n substitution. The first one is an example of a substitution constraint found by the algorithm, while the other two matrices are examples of discovered redundant constraints. Our method finds the $d(d+1)/2 = 6$ substitution constraints, and 14 redundant constraints similar to the two shown examples. For completeness, Figure 5 shows a compact representation of all the constraints for the \mathbf{y}_n substitution, where each row corresponds to one found basis vector (*i.e.*, the constraint matrix in half-vectorized form). We can see that all learned matrices are sparse and quantized, with nonzero values in $\{-1, \frac{1}{\sqrt{2}}, 1\}$.

We find that both substitutions lead to cost-tight and rank-tight relaxations when all constraints are imposed, with SVR above 10^9 and RDG below 10^{-4} . For the \mathbf{y}_n substitution,

¹³Here, we chose not to enforce the known constraint matrices using (14), to highlight the interpretability of the found constraints.

TABLE II: Overview of the tightened problems, including the variable groups, problem dimensions, and noise parameters. For simplicity, all substitutions are called z_i . N_{out} denotes the number of outliers, and noise levels correspond to the standard deviation of zero-mean Gaussian noise.

Problem	Parameters	Variables	Inlier noise (Outlier noise)
range-only localization	$d = 3, N_m = 10, N = 3$	$\{\{h, \theta_0\}, \{h, z_0\}, \{h, \theta_0, z_0\}, \dots\}$	10^{-2}
stereo-localization	$d \in \{2, 3\}, N = d + 1$	$\{\{h, \theta\}, \{h, z_0\}, \{h, \theta, z_0\}, \{h, z_0, z_1\}, \dots\}$	10^0
point-point registration [10]	$d = 3, N = 3$	$\{\{h, \theta\}\}$	10^{-2}
point-line registration [10]	$d = 3, N = 5$		10^{-3}
robust point-cloud registration [7]	$d = 3, N = 4, N_{\text{out}} = 1$	$\{\{h, \theta\}, \{h, \theta, w_0\}, \{h, \theta, z_0\}, \{h, \theta, w_0, w_1\}\}$	$10^{-2} (10^0)$
robust absolute pose estimation [7]	$d = 3, N = 6, N_{\text{out}} = 1$	$\{h, \theta, w_0, z_0\}, \{h, \theta, z_0, z_1\}, \dots\}$	$10^{-3} (10^{-1})$

TABLE III: Breakdown of characteristics for all tightened problems for the first stage of AUTOTEMPLATE. This stage has to be run only once, as the output are constraint templates. All times are in seconds, with t_n the total time to compute the nullspaces, t_a the time to apply templates to all variables, t_s the time to check for tightness, and t_r the time required to reduce the constraints using (25).

Problem	Dimensions n per iteration	# Constraints	# Sufficient	t_n [s]	t_a [s]	t_s [s]	t_r [s]	Total [s]	RDG	SVR
RO (z_n)	10 15	4	4	0.01	0.00	0.19	0.13	0.33	4.41e-05	1.76e+09
RO (y_n)	10 55	61	55	0.10	0.12	0.40	13.87	14.49	4.70e-05	2.30e+09
stereo (3D)	91 910 3250 9100	639	84	241.52	2.75	4.08	46.05	294.38	1.16e-06	1.96e+01
PPR	91	21	8	0.12	0.03	0.19	0.18	0.53	2.46e-06	8.93e+09
PPL	91	21	10	0.12	0.03	0.66	0.95	1.77	1.29e-04	8.68e+07
rPPR	91 105 325 120 351 703	1771	1554	5.99	10.87	24.58	588.93	630.37	7.52e-04	1.29e+00
rPLR	91 105 325 120 351 703	2349	1990	6.62	13.85	32.77	983.41	1036.65	1.54e-08	2.07e+01

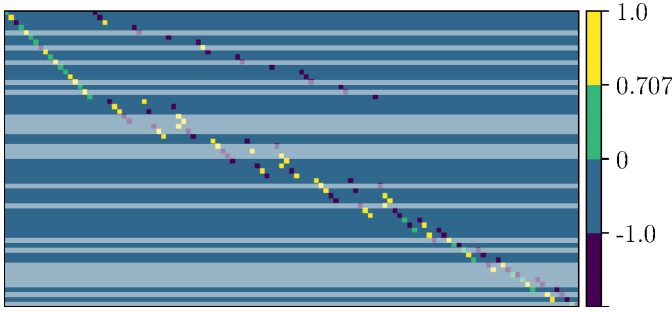


Fig. 5: Compact visualization of the learned constraint matrices for the y_n substitution of RO localization. Each row contains one basis vector, equivalent to the half-vectorized constraint matrix. Highlighted in dark are the sufficient constraints for rank-tightness.

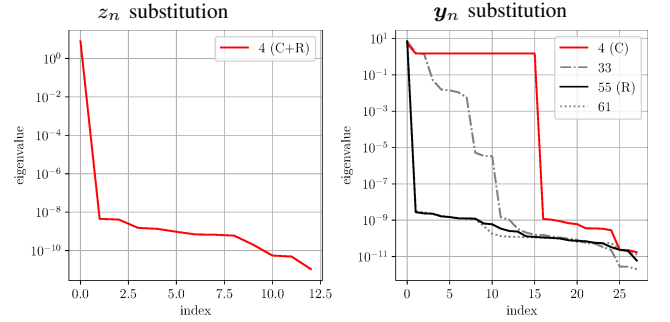


Fig. 6: Rank-tightness study for RO localization, using z_n substitution (left) vs. y_n substitution (right). We compare the spectra with different numbers of added constraints (gray lines), highlighting the points where cost-tightness (C) and rank-tightness (R) are obtained in red and black, respectively.

redundant constraints are required. Exactly which constraints are required and how they scale is investigated next.

3) Generating Scalable Constraints (AUTOTEMPLATE):

We have shown that the formulations with substitution y_n of the RO localization problem can be tightened, at least for a small problem. In this section, we show that the method can be generalized to problems of larger size. In this particular example, the learned constraints are interpretable, therefore we could infer the mathematical expression of all constraints, as we saw in Figure 4, and apply them to new setups (outcome 2 of Section IV-D). Instead, we show here that the algorithmic way of scaling up, which does not require any intermediate manual steps, is also tractable for larger problem sizes.

To generate scalable templates, we use AUTOTEMPLATE with the variable ordering given in Table II. The algorithm terminates after including variables $\{h, \theta_0, y_0\}$, at which point the found templates lead to a tight relaxation (in both cost and

rank) when applied to all $N = 3$ positions.¹⁴

Before applying the templates to new problems of increasing size, AUTOTEMPLATE reduces them to a sufficient subset of constraints using (25). Figure 6 visualizes this process, showing rank- and cost-tightness for different subsets of constraints used. First, we confirm that the substitution z_n leads to rank- and cost-tightness after adding the substitution constraints only. For y_n , when adding constraints one-by-one in the order dictated by (25), we find that 55 out of the 61 constraints are enough for rank-tightness. Cost-tightness, on the other hand, is achieved already after adding 4 constraints only.¹⁵

We generalize the templates required for rank-tightness to

¹⁴Note that we do not need to consider any combinations of positions (or substitutions), which is a consequence of the problem being separable. This could have been observed from (26), but we did not exploit this structure here to facilitate the extension to regularized problems (*i.e.*, with motion prior).

¹⁵It is expected that the reordering of constraints works for achieving cost-tightness faster, as this is what the Problem (25) is primarily designed to do. Faster rank-tightness is (if existent) merely a side-product of this process.

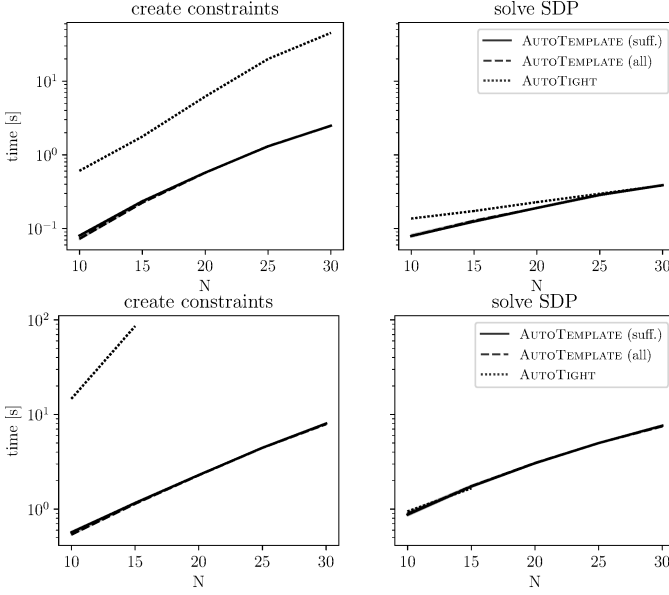


Fig. 7: Timing study for RO localization, using the z_n substitution (top) vs. the y_n substitution (bottom). We compare using only the sufficient (solid line) or all templates (dashed line) output by AUTOTEMPLATE, which are very close for this particular problem. They compare favorably to learning constraints from scratch for each problem using AUTOTIGHT.

problems with up to 30 positions. Figure 7 shows the time required for creating the constraints and solving the SDP for each problem size. We compare the processing times of learning the constraints for each problem from scratch using AUTOTIGHT, with using templates computed from AUTOTEMPLATE, using either all or only those sufficient for rank-tightness. Naturally, when using the substitution z_n , applying templates and checking for tightness remain relatively cheap as the problem size grows, because the number of total constraints grows only linearly in the number of variables. Even learning the constraints from scratch is reasonably fast for this case.

For the substitution y_n , however, AUTOTIGHT becomes prohibitively expensive beyond $N = 15$ positions. On the other hand, when using AUTOTEMPLATE, the cost of generating the constraints stays close to the cost of solving the SDP for all problem sizes. Ordering the constraints according to (25) did not have a significant effect in this case, and there is little difference between using all vs. only the sufficient constraints. Note that learning the templates and determining the sufficient subset constitute a fixed cost and are listed separately in Table III.

C. Stereo Localization

1) *Problem Statement:* In stereo localization, the goal is to estimate a stereo cameras' pose given the image coordinates, in both left and right frames, of a number of known landmarks. We call the known, homogenized landmarks \mathbf{m}_k with $k \in [N]$.¹⁶ For simplicity, we focus on one measurement

¹⁶We use N and not N_m because in stereo localization, the number of landmarks determines the problem size N (since the number of poses is fixed to one).

time only, and call the unknown pose at that time $\mathbf{T} \in SE(d)$, which contains both the rotation matrix from world to camera frame, $\mathbf{C} \in SO(d)$, and the associated translation $\mathbf{t} \in \mathbb{R}^d$. We collect the pixel measurements of landmark k in $\mathbf{y}_k^\top := [u_k^{(l)} \ v_k^{(l)} \ u_k^{(r)} \ v_k^{(r)}]$, where u and v denote the x and y coordinates in pixel space, and superscripts (l) and (r) correspond to the left and right frame, respectively. We call the intrinsic stereo camera matrix in d dimensions \mathbf{M}_d . For $d = 3$, we have:

$$\mathbf{M}_d = \begin{bmatrix} f_u & 0 & c_u & f_u \frac{b}{2} \\ f_v & c_v & 0 & 0 \\ f_u & 0 & c_u & -f_u \frac{b}{2} \\ f_v & c_v & 0 & 0 \end{bmatrix}, \quad (29)$$

where f_u , f_v , and b are the focal lengths and baseline, respectively. The forward measurement model is given by:

$$\mathbf{y}_k = \mathbf{M}_d (\mathbf{e}_d^\top \mathbf{T} \mathbf{m}_k)^{-1} \mathbf{T} \mathbf{m}_k, \quad (30)$$

where \mathbf{e}_d is the d -th standard basis vector. Given a number of pixel measurements from N landmarks, the pose can be estimated as the solution of the optimization problem

$$\min_{\mathbf{T} \in SE(d)} \sum_{k \in [N]} \|\mathbf{y}_k - \mathbf{M}_d (\mathbf{e}_d^\top \mathbf{T} \mathbf{m}_k)^{-1} \mathbf{T} \mathbf{m}_k\|^2. \quad (31)$$

Due to the $SE(d)$ constraint and the rational cost function, Problem (31) is hard to solve globally. However, the problem can again be lifted to a QCQP by introducing a series of relaxations and substitutions. First, we relax the $SO(d)$ to a $O(d)$ constraint, which essentially drops the $\det(\mathbf{C}) = 1$ constraint. As discussed in [5], this relaxation is often tight without additional constraints, and if not, handedness constraints can be added [10]. As we are automatically finding all redundant constraints, these constraints will be added later if required. Secondly, we can introduce the substitutions

$$\mathbf{v}_k := (\mathbf{e}_d^\top \mathbf{T} \mathbf{m}_k)^{-1} \mathbf{T} \mathbf{m}_k, \quad (32a)$$

$$\mathbf{u}_k^\top := [\mathbf{v}_k[1] \ \cdots \ \mathbf{v}_k[d-1] \ \mathbf{v}_k[d+1]], \quad (32b)$$

where in \mathbf{u}_k we have removed the d -th element of \mathbf{v}_k , which is always one by definition. Using \mathbf{v}_k , we obtain the following QCQP:

$$\begin{aligned} \min_{\mathbf{C}, \mathbf{t}} \quad & \sum_{k \in [N]} \|\mathbf{y}_k - \mathbf{M}_d \mathbf{v}_k\|^2 \\ \text{s.t.} \quad & (\mathbf{I}_d - \mathbf{v}_k \mathbf{e}_d^\top) \mathbf{T} \mathbf{m}_k = \mathbf{0}, \ k \in [N] \\ & \mathbf{C}^\top \mathbf{C} = \mathbf{I}_d, \end{aligned} \quad (33)$$

which we write as a homogeneous QCQP using the following lifted vector:

$$\mathbf{x}^\top = [h \ \mathbf{t}^\top \ \text{vec}(\mathbf{C})^\top \ \mathbf{u}_1^\top \ \cdots \ \mathbf{u}_N^\top]. \quad (34)$$

2) Determining Feasibility of Tightening (AUTOTIGHT):

As before, we first use AUTOTIGHT to investigate whether Problem (33) can be tightened. We use a small toy problem, choosing $N = d + 1$ landmarks.

The left plots of Figure 9 show the cost-tightness study for the 3D problem. Even when adding all 45 found constraints, the problem cannot be tightened in the present form. Note

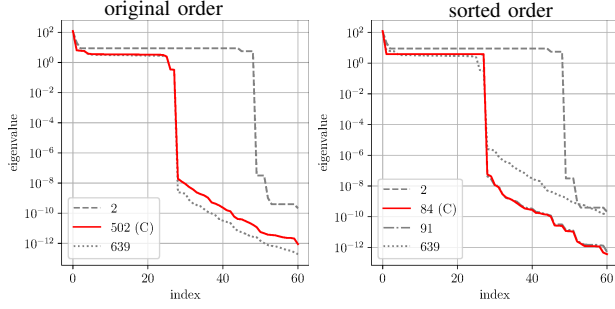


Fig. 8: Study of the singular value spectra of stereo localization using original order of constraints (left) and the sorted order using (25) (right). Even after adding the higher-order substitutions and all found redundant constraints, a significant number of eigenvalues are nonzero. More higher-order Lasserre variables may be required to achieve rank-tightness. See Figure 6 for a detailed description of the labels.

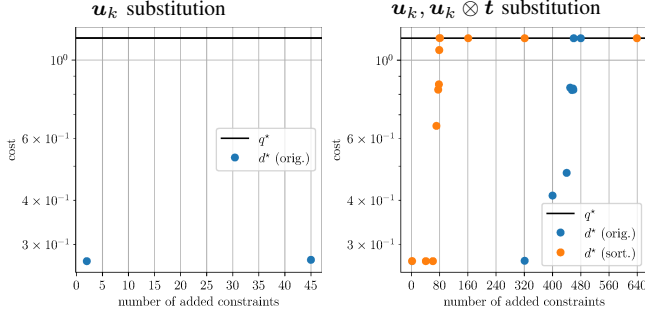


Fig. 9: Tightness study for stereo localization problem, using the original substitutions only (left) vs. the higher-order substitutions (right). We use a bisection algorithm on the number of added constraints, which immediately terminates when using the original substitutions as the problem is not cost-tight even when adding all possible constraints. When adding higher-order substitutions, tightness is achieved after a few steps.

how quickly we came to this conclusion: no manual search for redundant constraints had to be performed, a process that can be very time consuming.

We resort to (sparse) Lasserre hierarchy [13] to tighten the problem. We try different higher-order lifting functions and retest for tightness after adding all possible redundant constraints. We individually test additions such as $\mathbf{u}_k \otimes \mathbf{u}_k$, $\mathbf{t} \otimes \mathbf{t}$, etc. and find that by adding $(\mathbf{u}_k \otimes \mathbf{t})$ for each landmark, we achieve tightness. For simplicity, we call the combined substitution $\mathbf{z}_k^\top := [\mathbf{u}_k^\top (\mathbf{u}_k \otimes \mathbf{t})^\top] \in \mathbb{R}^{d+d^2}$. Figure 9 on the right shows the cost-tightness tests 3D, which now passes. Since cost-tightness is achieved, we can solve (25) to determine a significantly smaller subset of sufficient constraints: we reduce the number from 639 to 80 constraints, as shown in Figure 9 and Table III. In all considered cases, rank-tightness is not attained (see Figure 8) and may require additional lifting functions of even higher order. As we are already approaching what is computationally feasible for the SDP solver, we settle for cost-tightness for now.

3) Generating Scalable Constraints (AUTOTEMPLATE):

To scale this problem, it is crucial to use AUTOTEMPLATE, for two reasons. Firstly, the problem dimension is large, in particular after adding the additional lifting functions required for

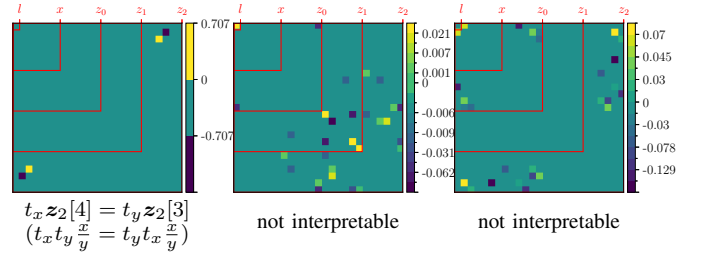


Fig. 10: Three learned constraint matrices for the 2D stereo localization problem. Many of the matrices are less sparse than in the range-only localization example and contain non-quantized numbers which suggests a dependency on landmark coordinates. Only few matrices, such as the one shown on the left, are interpretable (the identity is shown below the plot, where for simplicity, we call $\mathbf{t} = (t_x, t_y)^\top$, $\mathbf{Tm}_2 = (x, y, 1)^\top$, thus $\mathbf{u} = \frac{1}{y}(x, 1)^\top$ and $\mathbf{z}_2 = \frac{1}{y}(x, 1, t_x x, t_y x, t_x, t_y)^\top$).

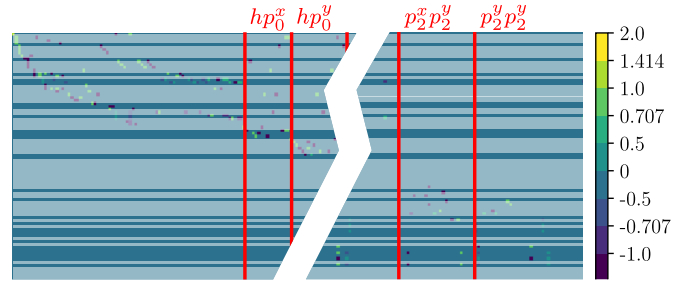


Fig. 11: Subset of the constraint templates learned for stereo-localization in 2D after factoring out parameters. The red bars delimit different parameter dependencies, with the left-most block corresponding to the original variables. Highlighted in dark are some of the sufficient templates for tightness (in total, 48 out of 170).

tightness. Secondly, an investigation of the learned constraints, shown in Figure 10, suggests that many matrices actually depend on the (known) landmark coordinates and therefore do not generalize to other setups.

As explained in Section V-B, we use as parameters that are (up to) quadratic polynomials of each landmark's coordinates. The succession of variable groups is listed in Table II. For each variable selection, we consider only the parameters touched by the considered variables. We achieve tightness after including all groups up to $\{h, z_0, z_1\}$. Figure 11 shows the output of the method (in compressed format), for the 2D example: a set of templates over not only the original variables, but also their products with the parameters. Most importantly, note that thanks to factoring out the parameters, the matrix is now more quantized, with all nonzero elements in $\{2, \sqrt{2}, \pm 1, \pm \frac{1}{\sqrt{2}}, \pm \frac{1}{2}\}$. We have thus eliminated the landmark dependencies and the obtained templates can be applied to any setup. The amount of constraints may seem unmanageable at first; but the templates can be significantly reduced by solving (25): only 48 of the 170 constraints (highlighted in dark in Figure 11) are sufficient for tightness.

We successfully apply the patterns for up to 30 landmarks, as shown in Figure 12. We show how the times to create constraints and solve the SDP scale with N , and report the one-time cost of finding the sufficient set of templates in

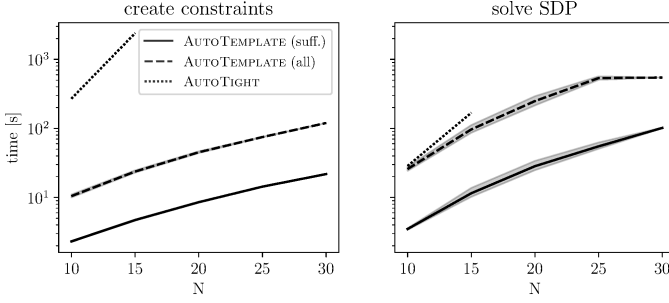


Fig. 12: Timing study of the stereo-localization problem in 3D as we increase the number of landmarks N . The labels are the same as in Figure 7. Learning constraints from scratch using AUTOTIGHT is prohibitively expensive even for $N = 10$. On the other hand, AUTOTEMPLATE scales reasonably up to $N = 30$.

Table III. As for RO localization, learning templates from scratch for each new setup does not scale beyond $N = 15$ landmarks, while applying the reduced templates comes at a reasonable cost, comparable to the cost of solving the SDP itself. This is a considerable improvement compared to existing approaches: inputting the same problem formulation to the (sparse) Lasserre hierarchy tool provided by [7] leads to unmanageable numbers of variables and constraints, even for small problem sizes. For $d = 3$ and only $N = 3$ landmarks, a total of 27,692 trivially satisfied constraints are generated, which is far beyond what SDP solvers can currently handle in reasonable time. In contrast, we can go to as many as $N = 30$ landmarks, at which point we compute 4,733 sufficient constraints for tightness.

D. Other Problems

We conclude the simulation study by applying the proposed method to a number of problems from the literature whose semidefinite relaxations have been shown to be tight using certain redundant constraints. As a starting point, we consider two multimodal registration problems that have been treated by Briaies *et al.* [10]: point-point registration (PPR) and point-line registration (PLR).

1) *PPR and PLR* [10]: In multimodal registration, the goal is to find an object's translation $\mathbf{t} \in \mathbb{R}^d$ and orientation $\mathbf{C} \in SO(d)$ w.r.t. a world frame, given measurements of points lying on the object. The object is assumed to be represented by a set of known geometric primitives of either points, lines, or planes. The problem is posed as the following minimization problem [10]:

$$\min_{\mathbf{C} \in SO(d), \mathbf{t} \in \mathbb{R}^d} \sum_{i=1}^N \|\mathbf{C}\mathbf{p}_i + \mathbf{t} - \mathbf{y}_i\|_{\mathbf{W}_i}^2, \quad (35)$$

with $\mathbf{p}_i \in \mathbb{R}^d$ the measured point and \mathbf{y}_i an arbitrary point on the associated primitive P_i (note that data association is assumed known). The matrix $\mathbf{W}_i \in \mathbb{R}^{d \times d}$ is chosen depending on the type of primitive P_i :

$$\mathbf{W}_i = \mathbf{I}_d \quad (\text{point}), \quad (36a)$$

$$\mathbf{W}_i = \mathbf{I}_d - \mathbf{v}_i \mathbf{v}_i^\top \quad (\text{line with unit direction } \mathbf{v}_i), \quad (36b)$$

$$\mathbf{W}_i = \mathbf{n}_i \mathbf{n}_i^\top \quad (\text{plane with normal } \mathbf{n}_i). \quad (36c)$$

a) *Manual method* [10]: Problem (35) can be relaxed to a QCQP by dropping the determinant constraint from $SO(d)$ as explained in Section VI-C, and introducing $\mathbf{x}^\top = [\mathbf{h} \quad \mathbf{t}^\top \quad \text{vec}(\mathbf{C})^\top]$. The rank relaxation of this QCQP was shown to be always tight when using the following set of constraints [10]:

$$\mathbf{h}^2 = 1 \quad (\text{prim., homogenization}), \quad (37a)$$

$$\mathbf{I}_d = \mathbf{C}^\top \mathbf{C} \quad (\text{prim., orthonormal rows}), \quad (37b)$$

$$\mathbf{I}_d = \mathbf{C} \mathbf{C}^\top \quad (\text{red., orthonormal columns}), \quad (37c)$$

$$\mathbf{c}_{i|3} \times \mathbf{c}_{i+1|3} = \mathbf{c}_{i+2|3}, i \in [3] \quad (\text{red., handedness}), \quad (37d)$$

where ‘‘prim.’’ and ‘‘red.’’ are short for primary and redundant, $|$ is the modulo operator and \mathbf{c}_i is the i -th column of \mathbf{C} . This leads to a total of $1 + 2 \cdot 6 + 3 \cdot 3 = 22$ constraints in 3D, accounting for the symmetry of the optimization variable.

b) *Proposed method*: Our method finds the required redundant constraints outlined above, but without any manual steps. Figure 13 shows the discovered constraint matrices (in compressed form) by AUTOTIGHT. We find a total of 21 independent constraints, including the homogenization, suggesting that at least one of the 22 constraints presented by [10] are linearly dependent. Indeed, looking at the orthonormality constraints, we observe that out of the $3 + 3$ constraints that touch the diagonal in (37b) and (37c), respectively, only 5 are linearly independent. To see this, let us call $h_i(\mathbf{C}) = 1$ the constraints touching the diagonal with $i \in \{1, 2, 3\}$ for (37b) and $i \in \{4, 5, 6\}$ for (37c). Then, it is easy to see that

$$\sum_{i=1}^3 h_i(\mathbf{C}) = \sum_{i=4}^6 h_i(\mathbf{C}), \quad (38)$$

so any of these six constraints can be written as a linear combination of the five others.

While these 21 constraints have been shown to be *sufficient* for tightness [10], they have not been shown to be *necessary*. In fact, we found that, for the considered noise level, none of the redundant constraints are required for PPR to be both cost- and rank-tight, as shown in Figure 14. For PLR, Figure 14 shows that the solution is in fact exactly rank two with only the seven primary constraints, but it becomes rank one after adding as few as two of the 12 available redundant constraints. Note that for this problem, we observed that the order of adding constraints did not make a difference.

2) *Robust estimation* [7]: Next, we consider two example problems treated by Yang *et al.* [7]: robust pointcloud registration and robust absolute-pose estimation. These two problems can in fact be seen as ‘robust’ variations of PPR and PLR, respectively, which is why we call them rPPR and rPLR, respectively.

Both rPPR and rPLR can be written in the form

$$\min_{\boldsymbol{\theta} \in \mathcal{D}} \sum_{i=1}^N \rho(r(\boldsymbol{\theta}, \mathbf{y}_i)), \quad (39)$$

where \mathcal{D} is the domain of $\boldsymbol{\theta}$, ρ is a robust cost function and r the residual function. It is shown in [7] that for a vast selection of robust cost functions, residual functions, and

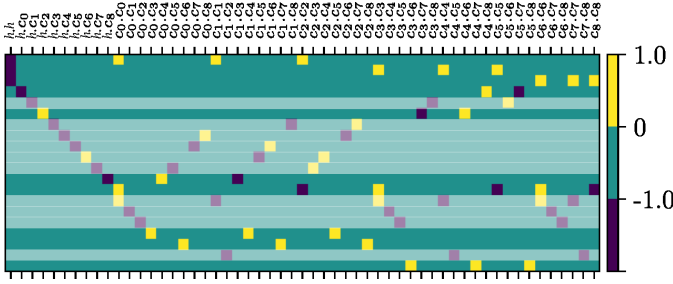


Fig. 13: Learned constraint templates for the multimodal registration problems [10]. The labels l and c_i correspond to the homogenization variable and the i -th element of $\text{vec}(\mathbf{C})$, respectively. We find that only 21 of the constraints suggested in [10] are actually linearly independent, see (38), and none of the redundant constraints are required for cost- and rank-tightness of point-point registration, while only a total of 10 (7 primary and 3 redundant) constraints, highlighted in dark, are required the point-line registration.

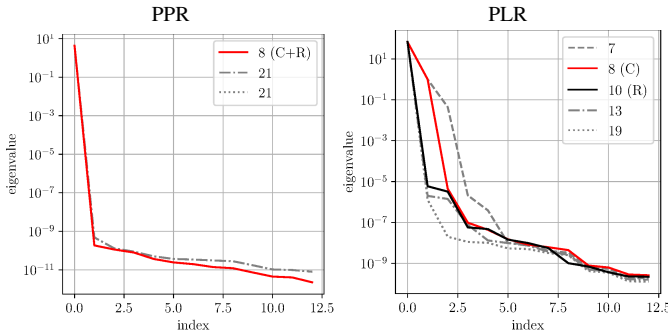


Fig. 14: Rank-tightness study for PPR (left) and PLR (right) problems [10]. Both problems are cost-tight without redundant constraints, and for PLR, only 2 redundant constraints are required for tightness; a small subset of the 12 available redundant constraints [10].

domains, Problem (39) can be written as a QCQP. As an example, we focus on the truncated least-squares (TLS) cost function in what follows. The residual functions are given by

$$\text{rPPR: } r(\boldsymbol{\theta}, \mathbf{y}_i) = \|\mathbf{C}\mathbf{p}_i + \mathbf{t} - \mathbf{y}_i\|^2, \quad (40)$$

$$\text{rPLR: } r(\boldsymbol{\theta}, \mathbf{y}_i) = \|\mathbf{C}\mathbf{p}_i + \mathbf{t}\|_{\mathbf{I}_d - \mathbf{v}_i \mathbf{v}_i^\top}^2. \quad (41)$$

In rPPR, \mathbf{p}_i and \mathbf{y}_i are matched measurements of a point-cloud observed from two different poses, while in rPLR, we assume \mathbf{p}_i to be known landmark coordinates, and \mathbf{v}_i unit vector measurements thereof, obtained for instance from a calibrated camera. The unknown state $\boldsymbol{\theta}$ is again the pose $\mathbf{t} \in \mathbb{R}^d, \mathbf{C} \in SO(d)$. In order to satisfy the Archimedian condition, the authors further restrict the domain \mathcal{D} to the domain with $\mathbf{t} \in \mathbb{R}^d$ contained in the ball of radius T .¹⁷ For the robust pose estimation problem, \mathbf{t} is also chosen so that the landmarks are in the field of view of the camera, characterized by aperture angle α . These two problems are thus examples with primary inequality constraints in (1).

a) *Manual method* [7]: For TLS cost, it has been shown that solving (39) is equivalent to solving [53]

$$\min_{\boldsymbol{\theta} \in \mathcal{D}, \mathbf{w} \in \{\pm 1\}^N} \frac{1}{2} \sum_{i=1}^N \frac{1 + w_i}{\beta_i^2} r^2(\boldsymbol{\theta}, \mathbf{y}_i) + 1 - w_i, \quad (42)$$

¹⁷The Archimedian condition is a stronger form of compactness [41].

where \mathbf{y}_i are measurements, \mathbf{w} is the vector of decision variables (for outliers, $w_i = -1$ and for inliers $w_i = 1$) and $\beta_i > 0$ are user-defined parameters determining the truncation threshold. Problem (42) can be written as a QCQP in the lifted vector

$$\mathbf{x}^\top = [h \quad \boldsymbol{\theta}^\top \quad \mathbf{w}^\top \quad \mathbf{z}^\top], \quad (43)$$

with $\boldsymbol{\theta}^\top = [\mathbf{t}^\top \text{vec}(\mathbf{C})^\top]$. The variable \mathbf{z} contains additional substitutions that are required to make Problem (42) quadratic in \mathbf{x} (the cost is cubic because the residual functions r are linear in $\boldsymbol{\theta}$). The authors propose to add the (sparse) Lasserre lifting function $\mathbf{z} = \boldsymbol{\theta} \otimes \mathbf{w}$, which leads to a tight relaxation after adding a list of (trivially satisfied) constraints. The authors also mention in passing that other lifting functions, such as $\mathbf{z} = \boldsymbol{\theta} \otimes \boldsymbol{\theta}$, which allow to write (42) as a QCQP, do not lead to a tight relaxation [7].

b) *Proposed method*: We study both lifting functions and come to the same conclusions as in [7]: both formulations allow for a large number of redundant constraints (which we found automatically), but only the second formulation becomes tight. Because of the large number of variables in the lifted state vector, we resort directly to AUTOTEMPLATE. The variable ordering used (for both problems) can be found in Table II. When using the lifting function $\mathbf{z} := \boldsymbol{\theta} \otimes \mathbf{w}$, the method terminates with cost-tightness after considering variables $\{l, \boldsymbol{\theta}, \mathbf{z}_0, \mathbf{z}_1\}$. For $\mathbf{z} := \boldsymbol{\theta} \otimes \boldsymbol{\theta}$, the method returns that no tightness can be achieved.

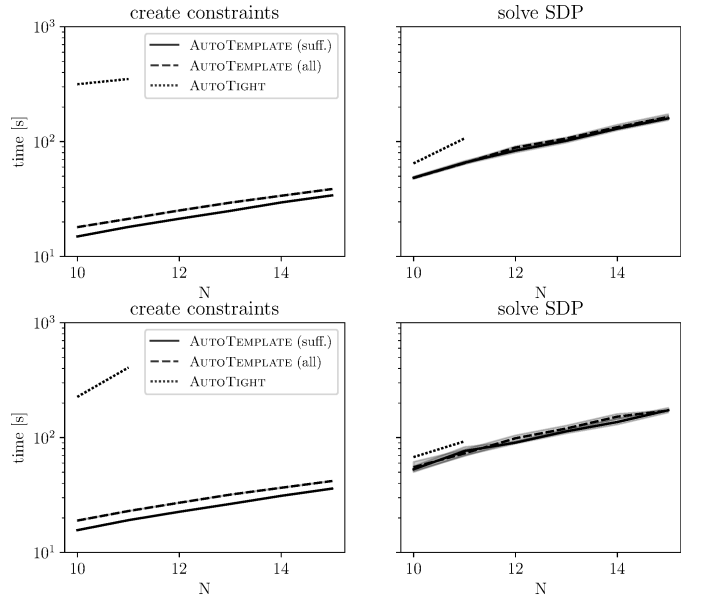


Fig. 15: Timing results of scaling to N landmarks for rPPR (top) and rPLR (bottom). Thanks AUTOTEMPLATE, we can automatically create the constraints of problems up to $N = 15$ landmarks.

The number of found and sufficient constraint templates can be found in Table III. We note that the number of required constraints is already very high when considering only $N = 4$ and $N = 6$ for rPPR and rPLR, respectively. Nevertheless, we can apply the templates to problems up to size $N = 15$, as shown in Figure 15. For both problems, learning constraints from scratch is prohibitively expensive. Thanks to AUTOTEMPLATE, we can use the templates instead,

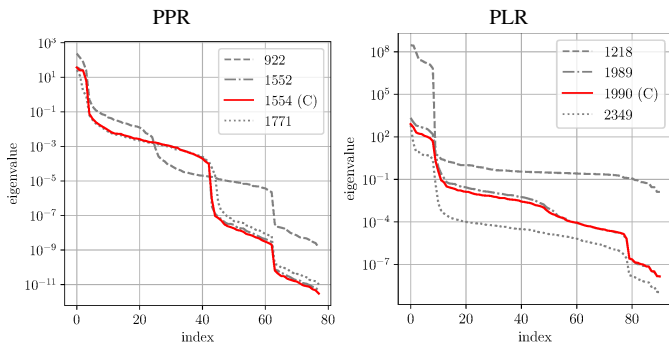


Fig. 16: Rank-tightness study for rPPR (left) and rPLR (right). We obtain cost-tightness, but not rank-tightness, for both problems.

TABLE IV: Comparison of the number of constraints found for rPPR and rPLR, respectively, using our method and the method proposed by [7], as a function of the number of measurements N .

N	rPPR		rPLR	
	our method	[7]	our method	[7]
10	4,508	6,257	5,330	7,379
11	5,293	7,398	6,279	8,724
12	6,139	8,633	7,304	10,180
13	7,046	9,962	8,405	11,747
14	8,014	11,385	9,582	13,425
15	9,043	12,902	10,835	15,214

and we obtain cost-tightness for all considered problems. Note that, just as in stereo localization, rank-tightness is not achieved and seems to not be computationally tractable since we already need many constraints for cost-tightness.

As a final study, we compare the number of constraints we find with the number of constraints found in [7] in Table IV. The results suggest that we find a significantly smaller subset of constraints, but without compromising tightness. One possible explanation is that we find more than only the “trivially satisfied” redundant constraints, thus we can choose from a larger pool when tightening the problem. We plan to further investigate this finding, taking a closer look at the nature of the found constraints.

VII. REAL-WORLD EXPERIMENTS

To conclude, we showcase the performance of the proposed framework on real-world datasets for RO localization and stereo-camera localization, respectively. The purpose of these experiments is to

- 1) clarify how to interface the simulation-based tightening methods with real-world datasets, and
- 2) investigate how the constraints, determined using a specific sampling function and noise level, generalize to real data with different characteristics.

A. Method

We first use AUTOTEMPLATE with random landmark placements to generate constraint templates. No knowledge of the actual measurement setup is required at this point. We then apply the templates to generate constraints, in each case using the actual landmark locations at each considered pose. One could also use the known landmarks for AUTOTEMPLATE, but

we show that even when using a generic sampler, the learned constraints generalize well.

B. Experimental Setups

We test our methods on two different experimental setups. The first dataset, called *starrynight* [54], includes stereo-camera images of Vicor markers scattered on the floor. The second dataset, called *STAR-loc* [55], includes stereo-camera images of *Apriltag* [56] landmarks scattered around a room at different heights and orientations. The *STAR-loc* dataset also includes UWB-based distance measurements to eight fixed landmarks, called anchors. Depictions of the two datasets are provided in Figure 17.

For RO localization, we always randomly select 4 out of the 8 available anchors to investigate the local minima that typically arise when anchors are almost co-planar. We report results on three example runs: *zigzag_s3*, *loop-2d_s4*, and *eight_s3*. For stereo localization, we only consider poses where more than 4 landmarks are observed, and we cap at maximum 8 landmarks, to limit the computation time.

C. Results

First, we investigate the tightness of the relaxations when evaluated on real data. Figure 18 shows the SVR and RDG for both RO and stereo localization, for randomly picked poses from both datasets (see Figure 17 for plots of the selected poses). We plot the respective tightness measures against the maximum residual error, which is a good proxy for the noise level and has been shown to affect the tightness of semidefinite relaxations [9, 39]. As expected, the relaxation of RO localization is mostly rank-tight across all considered datasets and poses, with an SVR of more than 10^6 for most poses. On the other hand, the stereo-localization relaxation is only reliably cost-tight for poses with a sub-pixel maximum residual error, which is a characteristic found in the *starrynight* dataset but in none of the runs from the *STAR-loc* dataset.

Next, we study the occurrence of local vs. global minima found in both problems. We certify a local solution by trying to find dual variables that satisfy (9) via a feasibility SDP. To account for numerical errors, we change (9a) to $|\mathbf{H}(\rho, \lambda)| \leq \epsilon \mathbf{1}$ and minimize ϵ as objective function. We claim a candidate solution \hat{x} is certified if we find a feasible solution with $\epsilon \leq 10^{-3}$.

Figure 19 shows the distribution of certified and uncertified solutions of RO and stereo localization, as a function of the maximum residual error. First, we note that local minima are ubiquitous for both problems, across all noise levels. Second, it can be observed that, as the noise increases, the global solution candidates from the stereo-localization problem are not all certified anymore, because of the lack of tightness at higher noise levels. However, local minima occur even at lower levels, and the relaxation can correctly identify them. For RO localization, all global solutions are correctly certified. All local solutions, which, compared to stereo localization, are harder to classify based on only their cost, are detected correctly. Note that since this relaxation is rank-tight, solving



Fig. 17: Experimental setups of real-world datasets. In the *starrynight* dataset [54], the visual landmarks are Vicor markers placed on the dark floor, and are captured with a stereo camera circling above them [54]. In the *STAR-loc* dataset [55], the visual landmarks are Apriltags placed at different heights and orientations, and are captured with a stereo camera moved along different trajectories through the room. The rig is also equipped with UWB tags that measure distances to 8 fixed anchors. The plots show the ground-truth poses at which stereo (top) and UWB (bottom) measurements are processed. The observed landmarks are depicted with black crosses.

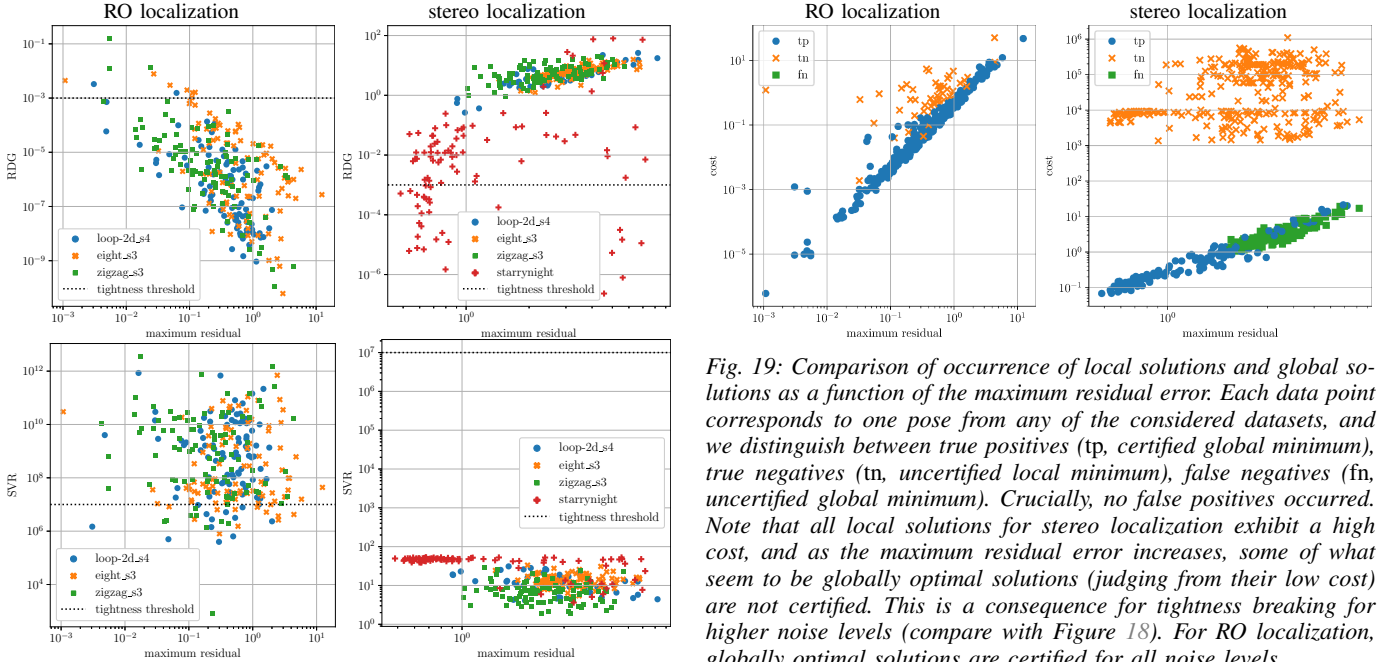


Fig. 18: Tightness study for RO localization (left plots) and stereo localization (right plots). Each data point corresponds to one estimated pose. Cost-tightness (top) and rank-tightness (bottom) are compared with the maximum residual error. The tightness thresholds are fixed to common values. We see that RO localization is mostly cost- and rank-tight, while stereo localization is only cost-tight for the lowest residual error levels in the *starrynight* dataset.

the primal SDP and extracting \mathbf{x}^* from the rank-1 \mathbf{X}^* would also be a viable solution method.

Finally, we show examples of local minima in Figure 20. For range-only localization, local minima typically occur when the anchors are in a degenerate configuration, such as almost coplanar. Intuitively speaking, the cost landscape nearly exhibits a symmetry in these situations and the local solver gets stuck in the wrong half when initialized there. For stereo localization, local minima occur more frequently and are typically completely off in terms of orientation, and were found to typically occur when initializing close to the wrong orientation.

To summarize, in both applications, initializing close to

Fig. 19: Comparison of occurrence of local solutions and global solutions as a function of the maximum residual error. Each data point corresponds to one pose from any of the considered datasets, and we distinguish between true positives (tp, certified global minimum), true negatives (tn, uncertified local minimum), false negatives (fn, uncertified global minimum). Crucially, no false positives occurred. Note that all local solutions for stereo localization exhibit a high cost, and as the maximum residual error increases, some of what seem to be globally optimal solutions (judging from their low cost) are not certified. This is a consequence of tightness breaking for higher noise levels (compare with Figure 18). For RO localization, globally optimal solutions are certified for all noise levels.

ground truth leads to the globally optimal solution, but without prior knowledge, random initializations and landmark placements are prone to yield bad, locally optimal solutions. For low-enough noise levels, we can certify globally optimal solutions since our formulation is tight when the automatically found redundant constraints are used.

VIII. CONCLUSION AND FUTURE WORK

We have presented new tools to find all possible redundant constraints for a given QCQP, which is paramount to tighten the semidefinite relaxations of many problems encountered in robotics. The first tool, AUTOTIGHT, allows for the fast evaluation of different problem formulations. We have successfully used this tool to evaluate different substitutions for range-only localization and find a novel tight formulation for stereo-based localization. The second tool, AUTOTEMPLATE, can then be employed to create scalable templates to tighten new

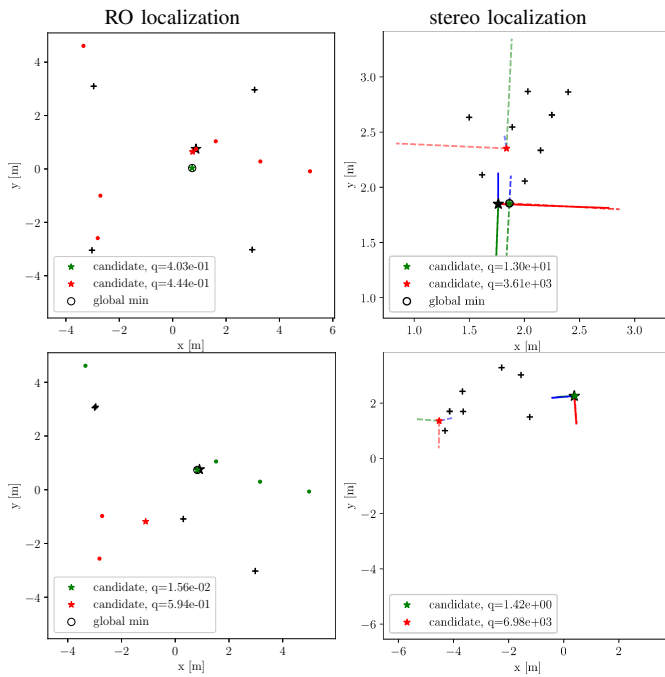


Fig. 20: Examples of local minima found in RO and stereo localization. The landmark locations are marked with black crosses and the ground truth with a black star. The solution candidates are marked with colored stars, and for RO localization, we also plot the respective initializations with dots of corresponding colors. Green stars are the local candidates with lowest cost, red are local candidates with higher cost and circled in black are certified global minima. For RO localization, all global solutions are correctly certified, and local minima occur when the anchors lie almost in one horizontal plane (top left) or vertical plane (bottom left). For stereo localization, the local minima have wrong orientation and, because of the lack of tightness at the high noise levels in STAR-loc, global minima cannot always be certified (e.g., bottom right). For starrynight, most global minima are certified (e.g., top right).

setups and larger problem sizes. To show the wide applicability of these tools, we have also evaluated their performance on example problems from the literature [10, 7], showing that we find tight relaxations with even fewer redundant constraints than previously considered. As SDPs scale poorly with the number of constraints, this is an important step to make semidefinite relaxations scale to general problems encountered in robotics.

A number of follow-up questions deserve further attention. First, it has been shown that both the measurement graph and the noise level can have an effect on tightness [39, 33, 4]. In future work, we plan to investigate these characteristics using the given tool, and in particular understand to what level the additional redundant constraints may push the boundaries of tightness. Along the same lines, a given measurement graph may in fact help in finding the variable substitutions and parameters that are most likely to succeed, a component of the proposed method that is currently defined by user input.

Finally, the full potential of the proposed method will be unlocked when faster SDP solvers are developed for problems that require redundant constraints. First steps into this direction have shown promising results [6, 7, 12], but more work remains to be done. In parallel, there lies potential in

further pushing the efficiency of optimality certificates of fast local solvers, for example using sampling-based approaches as in [18] or sparsity-exploiting approaches as in [33, 34].

REFERENCES

- [1] J. Rehder, J. Nikolic, T. Schneider, T. Hinzmann, and R. Siegwart, “Extending kalibr: Calibrating the extrinsics of multiple IMUs and of individual axes,” in *IEEE International Conference on Robotics and Automation (ICRA)*. Stockholm, Sweden: IEEE, 2016, pp. 4304–4311.
- [2] T. D. Barfoot, *State Estimation for Robotics*. Cambridge University Press, 2017.
- [3] J. Nocedal and S. J. Wright, *Numerical Optimization*, 2nd ed., ser. Springer Series in Operations Research. Springer-Verlag, 2006.
- [4] A. Papalia, A. Fishberg, B. W. O’Neill, J. P. How, D. M. Rosen, and J. J. Leonard, “Certifiably Correct Range-Aided SLAM,” *arXiv:2302.11614 [cs]*, 2023.
- [5] D. M. Rosen, L. Carlone, A. S. Bandeira, and J. J. Leonard, “SE-sync: A certifiably correct algorithm for synchronization over the special euclidean group,” *International Journal of Robotics Research*, vol. 38, no. 2-3, pp. 95–125, 2019.
- [6] H. Yang, L. Liang, L. Carlone, and K.-C. Toh, “An Inexact Projected Gradient Method with Rounding and Lifting by Nonlinear Programming for Solving Rank-One Semidefinite Relaxation of Polynomial Optimization,” *arXiv:2105.14033 [cs, math]*, no. arXiv:2105.14033, 2021.
- [7] H. Yang and L. Carlone, “Certifiably Optimal Outlier-Robust Geometric Perception: Semidefinite Relaxations and Scalable Global Optimization,” *IEEE Transactions on Pattern Analysis and Machine Intelligence*, vol. 45, no. 3, pp. 2816–2834, 2023.
- [8] H. Yang, J. Shi, and L. Carlone, “TEASER : Fast and certifiable point cloud registration,” *IEEE Transactions on Robotics*, vol. 32, no. 2, pp. 314–333, 2020.
- [9] A. Eriksson, C. Olsson, F. Kahl, and T.-J. Chin, “Rotation averaging and strong duality,” in *IEEE/CVF Conference on Computer Vision and Pattern Recognition (CVPR)*, 2018, pp. 127–135.
- [10] J. Briaies and J. Gonzalez-Jimenez, “Convex Global 3D Registration with Lagrangian Duality,” in *IEEE Conference on Computer Vision and Pattern Recognition (CVPR)*. Honolulu, HI: IEEE, 2017, pp. 5612–5621.
- [11] S. Boyd and L. Vandenberghe, *Convex Optimization*. Cambridge University Press, 2004.
- [12] J. Wang and L. Hu, “Solving Low-Rank Semidefinite Programs via Manifold Optimization,” *arXiv:2303.01722 [math]*, 2023.
- [13] J. B. Lasserre, “Global Optimization with Polynomials and the Problem of Moments,” *SIAM Journal on Optimization*, vol. 11, no. 3, pp. 796–817, 2001.
- [14] J. P. Ruiz and I. E. Grossmann, “Using redundancy to strengthen the relaxation for the global optimization of MINLP problems,” *Computers & Chemical Engineering*, vol. 35, no. 12, pp. 2729–2740, 2011.
- [15] A. Majumdar, R. Vasudevan, M. M. Tobenkin, and R. Tedrake, “Convex optimization of nonlinear feedback controllers via occupation measures,” *International Journal of Robotics Research*, vol. 33, no. 9, pp. 1209–1230, 2014.
- [16] L. Sun and Z. Deng, “Certifiably Optimal and Robust Camera Pose Estimation From Points and Lines,” *IEEE Access*, vol. 8, pp. 124 032–124 054, 2020.
- [17] J. Wang, V. Magron, and J.-B. Lasserre, “TSSOS: A Moment-SOS Hierarchy That Exploits Term Sparsity,” *SIAM Journal on Optimization*, vol. 31, no. 1, pp. 30–58, 2021.
- [18] D. Cifuentes and P. A. Parrilo, “Sampling algebraic varieties for sum of squares programs,” *SIAM Journal on Optimization*, vol. 27, no. 4, pp. 2381–2404, 2017.
- [19] C. Olsson, F. Kahl, and M. Oskarsson, “Branch-and-Bound Methods for Euclidean Registration Problems,” *IEEE Transactions on Pattern Analysis and Machine Intelligence*, vol. 31, no. 5, pp. 783–794, 2009.
- [20] R. Hartley, J. Trumpf, and D. H. Li, “Rotation averaging,” *International Journal of Computer Vision*, vol. 103, no. 3, pp. 267–305, 2013.
- [21] L. Brynte, V. Larsson, J. P. Iglesias, C. Olsson, and F. Kahl, “On the Tightness of Semidefinite Relaxations for Rotation Estimation,” *Journal of Mathematical Imaging and Vision*, vol. 64, no. 1, pp. 57–67, 2022.
- [22] J. Briaies, L. Kneip, and J. Gonzalez-Jimenez, “A Certifiably Globally Optimal Solution to the Non-minimal Relative Pose Problem,” in *IEEE/CVF Conference on Computer Vision and Pattern Recognition (CVPR)*. Salt Lake City, UT: IEEE, 2018, pp. 145–154.

- [23] D. Cifuentes, "A Convex Relaxation to Compute the Nearest Structured Rank Deficient Matrix," *SIAM Journal on Matrix Analysis and Applications*, vol. 42, no. 2, pp. 708–729, 2021.
- [24] K. Anstreicher and H. Wolkowicz, "On Lagrangian Relaxation of Quadratic Matrix Constraints," *SIAM Journal on Matrix Analysis and Applications*, vol. 22, no. 1, pp. 41–55, 2000.
- [25] E. Wise, M. Giamou, S. Khoubyarian, A. Grover, and J. Kelly, "Certifiably Optimal Monocular Hand-Eye Calibration," in *IEEE International Conference on Multisensor Fusion and Integration for Intelligent Systems (MFI)*, 2020, pp. 271–278.
- [26] J. Zhao, W. Xu, and L. Kneip, "A Certifiably Globally Optimal Solution to Generalized Essential Matrix Estimation," in *IEEE/CVF Conference on Computer Vision and Pattern Recognition (CVPR)*, 2020, pp. 12 034–12 043.
- [27] T. Marcucci, J. Umenberger, P. A. Parrilo, and R. Tedrake, "Shortest Paths in Graphs of Convex Sets," *arXiv:2101.11565 [cs, math]*, 2022.
- [28] T. Marcucci, M. Petersen, D. von Wrangel, and R. Tedrake, "Motion Planning around Obstacles with Convex Optimization," *arXiv:2205.04422 [cs]*, 2022.
- [29] S. Burer and R. D. Monteiro, "Local Minima and Convergence in Low-Rank Semidefinite Programming," *Mathematical Programming*, vol. 103, no. 3, pp. 427–444, 2005.
- [30] N. Boumal, "A Riemannian low-rank method for optimization over semidefinite matrices with block-diagonal constraints," *arXiv:1506.00575 [cs, math, stat]*, 2016.
- [31] K. J. Doherty, D. M. Rosen, and J. J. Leonard, "Performance Guarantees for Spectral Initialization in Rotation Averaging and Pose-Graph SLAM," *arXiv:2201.03773 [cs]*, 2022.
- [32] F. Dellaert, D. M. Rosen, J. Wu, R. Mahony, and L. Carlone, "Shonan rotation averaging: Global optimality by surfing $\{\text{SO}(p)\}$," in *European Conference on Computer Vision*, 2020, pp. 292–308.
- [33] C. Holmes and T. D. Barfoot, "An Efficient Global Optimality Certificate for Landmark-Based SLAM," *IEEE Robotics and Automation Letters*, vol. 8, no. 3, pp. 1539–1546, 2023.
- [34] F. Dümbgen, C. Holmes, and T. D. Barfoot, "Safe and Smooth: Certified Continuous-Time Range-Only Localization," *IEEE Robotics and Automation Letters*, vol. 8, no. 2, pp. 1117–1124, 2023.
- [35] Á. Parra, S.-F. Chng, T.-J. Chin, A. Eriksson, and I. Reid, "Rotation Coordinate Descent for Fast Globally Optimal Rotation Averaging," in *IEEE/CVF Conference on Computer Vision and Pattern Recognition (CVPR)*, 2021, pp. 4296–4305.
- [36] B. Buchberger, "An algorithm for finding the basis elements of the residue class ring of a zero dimensional polynomial ideal," Ph.D. dissertation, Johannes Kepler University of Linz, 1965.
- [37] S. Shen and R. Tedrake, "Sampling Quotient-Ring Sum-of-Squares Programs for Scalable Verification of Nonlinear Systems," in *IEEE Conference on Decision and Control (CDC)*, 2020, pp. 2535–2542.
- [38] MOSEK. ApS, *The MOSEK Optimization Toolbox for MATLAB Manual. Version 10.0.*, 2022.
- [39] D. Cifuentes, S. Agarwal, P. A. Parrilo, and R. R. Thomas, "On the local stability of semidefinite relaxations," *Mathematical Programming*, no. 193, pp. 629–663, 2022.
- [40] A. Beck, P. Stoica, and J. Li, "Exact and Approximate Solutions of Source Localization Problems," *IEEE Transactions on Signal Processing*, vol. 56, no. 5, pp. 1770–1778, 2008.
- [41] G. Blekherman, P. A. Parrilo, and R. Thomas, *Semidefinite Optimization and Convex Algebraic Geometry*. MOS-SIAM Series on Optimization, 2012, vol. 13.
- [42] T. F. Coleman and A. Pothén, "The Null Space Problem I. Complexity," *SIAM Journal on Algebraic Discrete Methods*, vol. 7, no. 4, pp. 527–537, 1986.
- [43] G. H. Golub and C. F. Van Loan, *Matrix Computations*, 4th ed. The John Hopkins University Press, 2003.
- [44] M. W. Mueller, M. Hamer, and R. D'Andrea, "Fusing ultra-wideband range measurements with accelerometers and rate gyroscopes for quadcopter state estimation," in *IEEE International Conference on Robotics and Automation (ICRA)*, 2015, pp. 1730–1736.
- [45] A. Goudar, W. Zhao, T. D. Barfoot, and A. P. Schoellig, "Gaussian Variational Inference with Covariance Constraints Applied to Range-only Localization," in *IEEE/RSJ International Conference on Intelligent Robots and Systems (IROS)*, 2022, pp. 2872–2879.
- [46] F. Zafari, A. Gkelias, and K. K. Leung, "A Survey of Indoor Localization Systems and Technologies," *IEEE Communications Surveys & Tutorials*, vol. 21, no. 3, pp. 2568–2599, 2019.
- [47] L. Matthies and S. Shafer, "Error modeling in stereo navigation," *IEEE Journal on Robotics and Automation*, vol. 3, no. 3, pp. 239–248, 1987.
- [48] G. Terzakis and M. Lourakis, "A Consistently Fast and Globally Optimal Solution to the Perspective-n-Point Problem," in *European Conference on Computer Vision*, A. Vedaldi, H. Bischof, T. Brox, and J.-M. Frahm, Eds., 2020, pp. 478–494.
- [49] S. Diamond and S. Boyd, "CVXPY: A Python-Embedded Modeling Language for Convex Optimization," *Journal of Machine Learning Research*, vol. 17, pp. 1–5, 2016.
- [50] A. Agrawal, R. Verschueren, S. Diamond, and S. Boyd, "A rewriting system for convex optimization problems," *Journal of Control and Decision*, vol. 5, no. 1, pp. 42–60, 2018.
- [51] J. Townsend, N. Koep, and S. Weichwald, "Pymanopt: A Python Toolbox for Optimization on Manifolds using Automatic Differentiation," *Journal of Machine Learning Research*, vol. 17, no. 137, pp. 1–5, 2016.
- [52] C. Liu and N. Boumal, "Simple algorithms for optimization on Riemannian manifolds with constraints," *arXiv:1901.10000 [math]*, 2019.
- [53] M. J. Black and A. Rangarajan, "On the unification of line processes, outlier rejection, and robust statistics with applications in early vision," *International Journal of Computer Vision*, vol. 19, no. 1, pp. 57–91, 1996.
- [54] T. D. Barfoot, "State Estimation for Aerospace Vehicles - AER1513 Course Assignments," *University of Toronto Institute for Aerospace Studies*, 2011.
- [55] "STAR-loc: Dataset for STereo And Range-based localization," <https://github.com/duembgen/starloc>.
- [56] J. Wang and E. Olson, "AprilTag 2: Efficient and robust fiducial detection," in *IEEE/RSJ International Conference on Intelligent Robots and Systems*, 2016, pp. 4193–4198.